[American Journal of Science, Vol. 309, January, 2009, P. 1–42, DOI 10.2475/01.2009.01]

American Journal of Science

JANUARY 2009

THE LATE MIOCENE THROUGH PRESENT PALEOELEVATION HISTORY OF SOUTHWESTERN TIBET

J. E. SAYLOR*,†, J. QUADE*, D. L. DETTMAN*, P. G. DeCELLES*, P. A. KAPP*, and L. DING**

ABSTRACT. Recent research using stable isotopes of carbon and oxygen from carbonates and fossil teeth seems to support both a pre- and post-mid-Miocene uplift of the southern Tibetan Plateau. We examined this issue by analysis of well-preserved fossil mollusks and plant remains from the Zhada Basin in southwestern Tibet, which ranges in age from ~ 9.2 to <1 Ma. Based on $\delta^{18}O_{cc}$ values from shell aragonite, we estimate that oxygen isotope ratios of Miocene – Pleistocene paleo-surface water ($\delta^{18}O_{psw}$) in Zhada Basin ranged from –24.5 to –2.2‰ (VSMOW). The lowest of these calculated values are lower than $\delta^{18}O_{sw}$ values [–17.9 to –11.9‰ (VSMOW)] of modern water in the basin. The extremely low $\delta^{18}O_{psw}$ values from fluvial mollusks and evaporatively elevated $\delta^{18}O_{psw}$ values from lacustrine mollusks, show that the peaks surrounding the Zhada Basin were at elevations at least as high as, and possibly up to 1.5 km higher than today, and that conditions have been arid since at least 9 Ma. A decrease in elevation since the Miocene is not specifically predicted by any existing mechanical models for the development of the Tibetan Plateau.

Paleoenvironmental modeling and physical evidence shows that the climate in Zhada Basin was cold and arid, indistinguishable from modern. The $\delta^{13}C_{pm}$ values of well-preserved vascular plant material increase from −23.4 to –26.8 permil at the base of the Zhada Formation to as high as −8.4 permil above 250 to 300 m. This shift denotes the expansion of C_4 biomass in this high, arid watershed at ~ 7 Ma, and thus corresponds to the C_3 – C_4 transition observed in Neogene deposits of the northern Indian sub-continent.

INTRODUCTION

The Tibetan Plateau occupies the center of the largest continent – continent collision on Earth and yet is actively undergoing extension (for example, Molnar and Tapponnier, 1978; Armijo and others, 1986; Taylor and others, 2003). Models invoked to explain the development of the Tibetan Plateau drive our thinking about convergent orogens worldwide. These models make predictions about the elevation history of the plateau (for example Armijo and others, 1986; Molnar and others, 1993; Ratschbacher and others, 1994; Murphy and others, 1997; McCaffrey and Nabelek, 1998; Seeber and Pecher, 1998; Tapponnier and others, 2001; DeCelles and others, 2002; Beaumont and others, 2004; Kapp and Guynn, 2004; Guynn and others, 2006; Rowley and Currie, 2006). In addition, numerous studies have linked elevation changes on the Tibetan Plateau to changes in precipitation, aridity, and large-scale oceanic and atmospheric circulation patterns (for example, Kroon and others, 1991; Raymo and Ruddiman, 1992; Molnar and others, 1993; Quade and others, 1995; Ruddiman and others, 1997; Dettman and others, 2001; Zhisheng and others, 2001; Molnar, 2005). Understanding what drove the Tibetan Plateau to high elevations, and whether those

*Department of Geosciences, University of Arizona, Tucson, Arizona 85721, USA, (520) 621-2672
**Institute of Tibetan Plateau Research, Chinese Academy of Sciences, P.O. Box 2871, Beijing, China 100029
†Corresponding author's present address: Department of Geological Sciences, Jackson School of Geosciences, The University of Texas at Austin, Austin, Texas 78712-0254; jsaylor@mail.utexas.edu

elevations are long lived and stable, is fundamental to understanding the interaction between asthenospheric, lithospheric and climatic processes.

In this paper we present a Miocene – Pleistocene sedimentary record in the Zhada Basin in southwestern Tibet, representing the first paleoelevation study in western Tibet. The sediments are rich in well-preserved gastropod shells and plant organic matter. From these archives, we have produced a detailed paleoelevation and paleoenvironmental record. The oxygen isotopic composition of the shells allows us to reconstruct mean watershed elevation through time, after accounting for the major variables that affect the oxygen isotopic system in both the modern and ancient record. The oxygen record shows that Zhada Basin was arid since the late Miocene, and that this part of the Tibetan Plateau stood as high as today, and possibly higher. The carbon record from plant remains shows that C_4 plants expanded across at least parts of this high watershed during the late Miocene. The C_4 plant expansion at this time agrees with observations from the Gyirong Basin and Thakkhola graben in south-central Tibet and Miocene Siwalik Group deposits in northern Pakistan and Nepal (Quade and others, 1995; Garzione and others, 2000a; Wang and others, 2006).

Previous Paleoelevation Work

There is still not unanimity within the scientific community regarding how to interpret the many complex proxies for Tibetan Plateau paleoelevation (for example, Molnar, 2005) despite more than two decades of research on the topic. The earliest work on Tibetan paleoelevation indicated a late Miocene or more recent uplift based on fossil, sedimentological, and structural data (for example, Liu, 1981; Zhang and others, 1981; Li and others, 1986; Zheng and others, 2000; Li and Zhou, 2001). Quade and others (1995) used a change from C_3 to C_4 dominated vegetation in the Himalayan foreland to argue for initiation or strengthening of the Asian monsoon at about 7 Ma. They linked the change in vegetation to Himalayan or Tibetan Plateau uplift, insofar as summertime heating of the air above the high Tibetan Plateau drives current monsoon circulation. This hypothesis was strengthened by the work of Kroon and others (1991), Prell and Kutzbach (1992), and Prell and others (1992), which linked increased upwelling in the Arabian Sea at 7.4 to 8 Ma to onset or strengthening of the Asian monsoon.

Evidence developed more recently both supports and contradicts the idea of relatively recent (late Miocene or later) uplift of the Tibetan Plateau. Early in the debate, Turner and others (1993) reported late-Miocene, potassium-rich lavas in northern Tibet. Turner and others (1993) and Molnar and others (1993) used this to argue for gravitational removal of thickened lithosphere and, by inference, uplift of the Tibetan Plateau. However, subsequent documentation of widely distributed volcanism of Eocene – Miocene age across the plateau (Chung and others, 1998; Wang and others, 2001; Ding and others, 2003) rendered the previous line of evidence more ambiguous. Dettman and others (2001) argued for an onset of the Asian monsoon by 10.7 Ma by showing that bivalves from the Himalayan foreland show evidence for seasonal oscillations between wet and very arid conditions, implying that a strong monsoonal circulation was in place between 10.7 and 3Ma. Even the occurrence of normal faulting on the Tibetan Plateau, once thought to mark attainment of high elevations at around 8 Ma (for example Harrison and others, 1992), has been shown to extend to at least the mid-Miocene (for example, Blisniuk and others, 2001).

Recent paleobotanical and stable isotope studies, focused primarily on south-central Tibet, generally point to high elevations in this region since the Eocene – Oligocene. The earliest quantitative paleoelevation studies on paleosol carbonate, lacustrine micrite and fossil shells obtained very low $\delta^{18}O$ values, indicating high elevations since 10 to 11 Ma in Thakkhola graben (Garzione and others, 2000a; Rowley and others, 2001), since $\sim$ 8 Ma in Gyirong Basin (Rowley and others, 2001) and since 15 Ma in the Oiyug Basin (Currie and others, 2005). The latter was confirmation of an

earlier leaf physiognomy study in the Namling Basin which also indicated high elevations (Spicer and others, 2003). Stable isotope studies in the Lunpola Basin (Rowley and Currie, 2006), Nima Basin (DeCelles and others, 2007), and the Tarim and Qaidam Basins (Graham and others, 2005) argued for high elevations on the Tibetan Plateau back to at least the Oligocene.

Wang and others (2006) recently reinvigorated the argument for a post-mid-Miocene uplift of the southern Tibetan Plateau by presenting carbon isotope data from 7 Ma mammal fossils in the Gyirong Basin (present elevation: 4,200 m, ~600 km east of the Zhada Basin) demonstrating that C_4 plants composed a significant fraction of their diet. As C_4 grasses today are apparently rare above 3,000 m (Wang, 2003; Lu and others, 2004), Wang and others (2006) concluded that the southern Tibetan Plateau attained its current elevation within the last 7 million years. However, there is some evidence that C_4 plants are present at high elevations on the Tibetan Plateau (Garzione and others, 2000a; Wang and others, 2008b). The results of paleoelevation studies to date constitute an important beginning to a still spatially and temporally limited picture of Tibetan uplift. In this paper, we present the first paleoaltimetry study from western Tibet and address the conflicting conclusions from stable isotope and paleoenvironmental studies.

OXYGEN ISOTOPE PALEOALTIMETRY

Oxygen isotope analysis has emerged as a powerful tool for reconstructing paleoelevations (for example, Siegenthaler and Oeschger, 1980; Chamberlain and Poage, 2000; Dettman and Lohmann, 2000; Garzione and others, 2000a, 2000b; Poage and Chamberlain, 2001; Currie and others, 2005; Cyr and others, 2005; Rowley and Currie, 2006; Rowley and Garzione, 2007). The underlying principle of these reconstructions is that oxygen or deuterium isotopic compositions of meteoric water (expressed as $\delta^{18}O_{mw}$ or δD_{mw}, respectively, in units ‰) vary as a function of elevation, decreasing by global average values of about –2.8 ‰/km (Poage and Chamberlain, 2001). In the ideal case, the $\delta^{18}O$ value of surface water and minerals precipitated from that water reflect the average $\delta^{18}O_{mw}$ value of rainfall in the catchment. The details of oxygen isotope paleoaltimetry are presented in reviews by Blisniuk and Stern (2005), and Rowley and Garzione (2007). In brief, the following factors must be accounted for before drawing conclusions about paleoelevation and paleoclimate from stable isotope data: (1) comparison with modern water to establish the modern lapse rate, (2) proof against diagenesis, and (3) correction for climate change. The third factor includes identifying and assessing changes in the source region, the amount effect, temperature, and the pathway of relevant air masses. Reliable age control must also be established before drawing tectonic implications from paleoelevation reconstructions.

REGIONAL SETTING OF ZHADA BASIN

The Zhada Basin is a late-Cenozoic sedimentary basin located just north of the high Himalayan ridge crest in the west-central part of the orogen (~30° N, 80° E, fig. 1A). The axis of the basin is parallel to the general arc of the Himalaya which, in this location, is approximately northwest-southeast. The current outcrop extent of the basin fill is approximately 9,000 km^2. The sedimentary basin fill is undisturbed and lies in angular or buttress unconformity with underlying deformed Tethyan Sedimentary Sequence (TSS) strata that were previously shortened in the fold-thrust belt. After deposition, the Sutlej River incised through to the basement, exposing the entire basin fill in a spectacular series of canyons and cliffs. The presence of a basin above the TSS in this location is in contrast to much of the Himalaya where the TSS caps some of the highest mountains in the world, including Mount Everest.

The Zhada Basin is bounded by the South Tibetan Detachment System (STDS) to the southwest, the Indus Suture to the northeast, and the Leo Pargil/Qusum and Gurla Mandhata gneiss domes to the northwest and southeast, respectively (fig. 1B). The STDS is a series of north-dipping, low-angle, top-to-the-north normal faults which

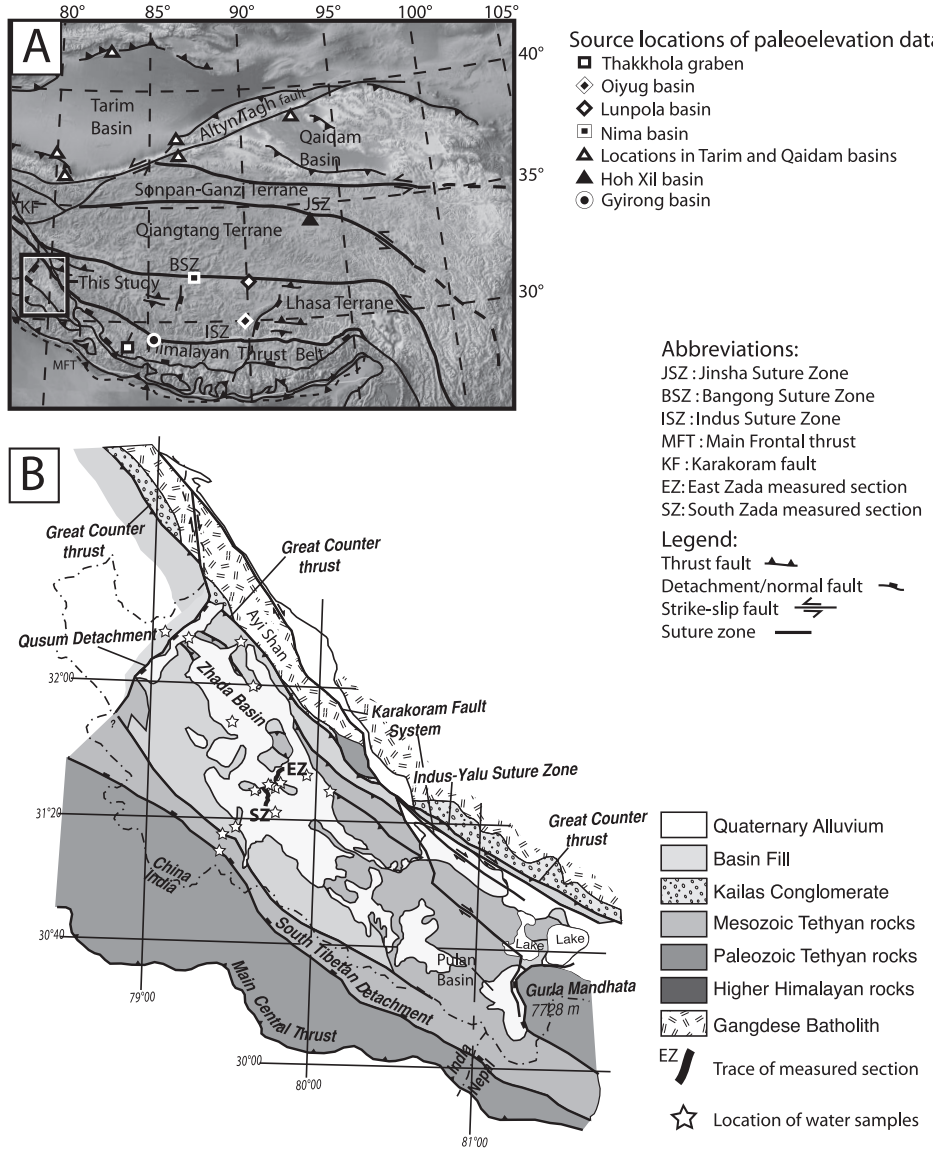

Fig. 1. (A) Elevation, shaded relief and generalized tectonic map of the Himalayan – Tibetan orogenic system showing the location of the Zhada Basin relative to other sources of paleoelevation data on the plateau. Sources for paleoelevation data are as follows; Thakkhola graben: Garzione and others (2000b), Oiyug basin: Currie and others (2005) and Spicer and others (2003), Lunpola basin: Rowley and Currie (2006), Nima basin: DeCelles and others (2007), locations in the Tarim and Qaidam basins: Graham and others (2005), Hoh Xil basin: Cyr and others (2005) and Gyirong basin: Rowley and others (2001) and Wang and others (2006). Image from the UNAVCO Jules Verne Voyager and the Generic Mapping Tools (GMT). (B) Generalized geologic map of the Zhada region. Gastropod samples for this study come from measured sections whose location is indicated by solid black lines. Modified from published mapping by Chen and Xu (1987), Murphy and others (2000, 2002) and unpublished mapping by M. Murphy.

place low-grade Paleozoic – Mesozoic metasedimentary rocks on high-grade gneisses and granites of the Greater Himalayan sequence. No ages for movement on the STDS in this area have been published, but elsewhere in the orogen ages range from 21 to 12 Ma (Murphy and Yin, 2003). Although rocks of Indian affinity are separated from

those of Asian affinity by the Indus Suture, the region north of the STDS is considered the southern edge of the Tibetan plateau for this study because it is hydrologically integrated with areas north of the Indus Suture. In the Zhada Basin region the Oligo-Miocene Great Counter Thrust, a south-dipping, top-to-the-north thrust system, modifies the Indus Suture (for example, Ganser, 1964; Yin and others, 1999). Exhumation of the Leo Pargil/Qusum and Gurla Mandhata gneiss domes (fig. 1B) by normal faulting initiated at ~ 16 Ma and 9 Ma, respectively (Murphy and others, 2002; Thiede and others, 2006) and is ongoing today. The unique setting of Zhada Basin makes it an ideal place to test hypotheses about climate, tectonics and paleoelevation in the Himalaya and southwestern Tibet.

We measured 14 stratigraphic sections covering the basin extent from the Zhada county seat in the southeast to the Leo Pargil/Qusum range front in the northwest (fig. 1B). The basin fill consists of approximately 800 m of fluvial, lacustrine, aeolian and alluvial fan deposits and is divided broadly into 3 intervals (fig. 2A).

1) The lower part of the section consists of ~ 200 m of trough cross-bedded sandstone and well-organized, imbricated pebble to cobble conglomerate. Broadly lenticular bodies of sandstone and conglomerate are interpreted as channel fills. The presence of 3 to 4 m thick bar foresets and channel forms suggests the presence of deep channels and large mid-channel macroforms. We interpret these as fluvial deposits laid down by large-scale rivers ancestral to the Sutlej or Indus, based on provenance and paleocurrent orientation data. Interbedded with these lithofacies are fine-grained, laminated sandstone and siltstone layers showing extensive soft-sediment deformation. These units contain abundant mammal, gastropod and plant fossils. We interpret these fine-grained intervals as marshy bog or overbank deposits within a low-gradient fluvial setting.

2) The approximately 250 m thick middle unit consists of an upward coarsening succession of cycles. Individual cycles are up to 17 m thick, coarsen upward, and contain profundal lacustrine claystone in their lower part and deltaic and wave-worked sandstone and conglomerate in their upper part. The claystone is devoid of macrofossils but the sandstone often has well-preserved, robust gastropod shells. Evidence of desiccation episodes, including gypsum layers and mudcracked mud-flat facies, is also present in the middle unit interval. Upward coarsening cycles are interpreted as progradational lacustrine sequences.

3) The upper 350 m of the Zhada Formation continues the upward coarsening progression displayed in the middle unit but becomes much coarser. The profundal claystone facies is replaced by deltaic or lake margin deposits. Individual parasequences contain lake-margin and alluvial-fan and fan-delta conglomerates.

METHODS AND MATERIALS

Age Control

We sampled the entire thickness of two measured sections and a portion of a third for magnetostratigraphic analysis, for a total sampling thickness of ~ 1400 m. We collected 4 to 5 samples from 184 sites (102 from the South Zhada section, 5 from the East Zhada section, and 77 from the Southeast Zhada section) using a cordless, hollow-bit drill using standard paleomagnetic sampling techniques (Butler, 1992). Samples were stored in a magnetically shielded room (~300 nT background field) housing the cryogenic magnetometer and demagnetization equipment, for at least 72 hours prior to measurement of natural remnant magnetization (NRM) and throughout the analysis process. We measured NRM using a 2G Model 755R three-axis cryogenic magnetometer with in-line degaussing system and automated sample handler. All cores were analyzed prior to any heating to isolate NRM. Using furnaces with programmable temperature controllers and ten thermocouple temperature sensors on each sample rack, we thermally demagnetized one sample from each site with

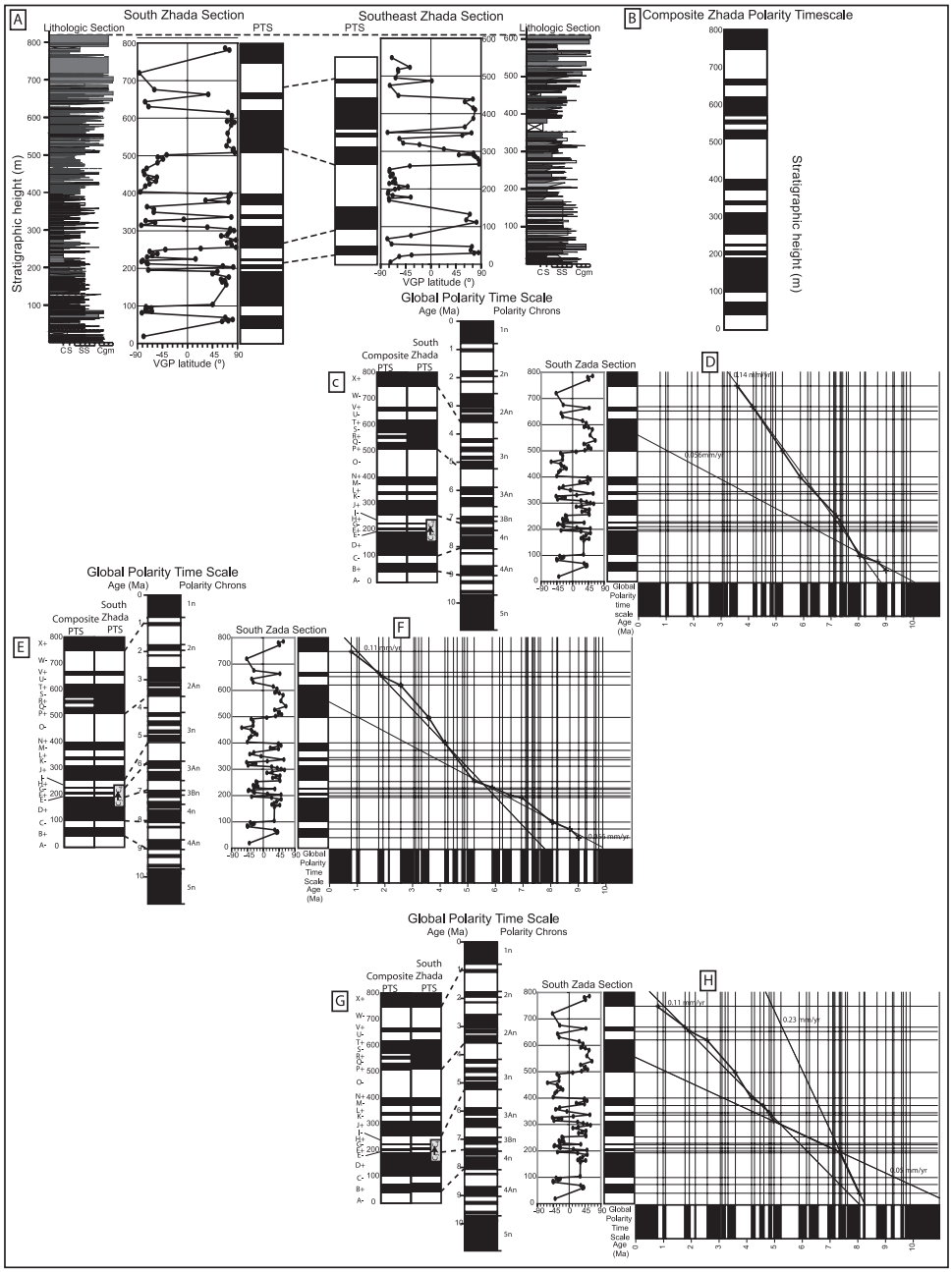

Fig. 2. Measured sections and magnetostratigraphic results for the South Zhada and Southeast Zhada sections. Sections were correlated using the top surface as a datum (A) to produce a composite magnetostratigraphic column (B). Which was then correlated with the GPTS of Cande and Kent (1995) (C-H). Our favored correlation is E. See text for details. 91 sites were used to construct the South Zhada section and 60 sites were used to construct the Southeast Zhada section.

temperature steps as follows: 50 degree steps from 100 to 300°C, 20 degree steps from 300 to 400°C and 20 degree steps from 500 to 700°C. We based temperature steps for subsequent batches on these initial results. Temperature steps within 100 degrees of

the Curie temperature were 20 degrees for all batches (see Appendix fig. A1 for representative vector diagrams). Characteristic Curie temperatures were between 580 °C and 700°C, indicating that magnetite and hematite were the primary carriers of characteristic remnant magnetization (ChRM). However, magnetic intensity in a minority of the samples decreased markedly by 300°C, indicating the possible presence of goethite.

The principle component analysis was done using the origin as a separate data point ["origin" line fit of Butler (1992)] and using at least 4 temperature steps. We discarded samples with line fits yielding a maximum angular deviation of >15° from further analyses. We then plotted site averages for sites with samples that passed the maximum angular deviation test on an equal area stereonet and calculated mean vectors for normal and reversed sites. The mean vectors for both the South Zhada and Southeast Zhada measured sections were antiparallel and thus passed the reversals test (see Appendix fig. A2, Butler, 1992).

Most samples show essentially univectoral decay of NRM toward the origin of the vector endpoint diagram. In order to eliminate potentially inaccurate results, we divided the sample set into quality sets A, B, C, and D (fig. A1). Sites with > 3 samples which passed the maximum angular deviation test and with a site-mean clustering of ChRM which yielded a 95 percent confidence limit (α_{95}) ≤ 15° and K ≥ 30 were then designated class A sites. Sites with ≥3 samples and with a site-mean clustering of ChRM which yielded a 95 percent confidence limit (α_{95}) > 15° were designated class B sites. Sites with 2 samples which yielded consistent inclinations and declinations were designated class C sites. Sites with only 1 sample which passed the maximum angular deviation test or with 2 samples which yielded inconsistent inclinations or declinations were not included in the magnetostratigraphic column (D sites). We constructed the resultant magnetostratigraphic columns from 87 class A sites, 60 class B sites and 7 class C sites. Magnetic reversals were placed mid-way between adjacent data points with opposite polarities. The placement of some reversals based on a single site is warranted given our caution in processing multiple samples from each site and discarding sites where data were suspect.

Modern Water

We collected 28 water samples at 20 locations throughout Zhada Basin (fig. 1B, Appendix table A1), providing the densest sampling coverage for any area in Tibet outside of Lhasa. Several sites were resampled during consecutive years. Samples were collected from a number of different settings ranging from the Sutlej main stem to small seep springs at the base of the Zhada Formation. Virtually no local rain fell during the sampling campaigns, meaning we were sampling higher elevation run-off. ArcGIS was used to delineate watersheds for each of our samples. This allowed calculation of the average elevation at which precipitation feeding these streams and springs fell by obtaining hypsometric mean watershed elevations for each sample. This approach is consistent with the work of Garzione and others (2000b), Rowley and others (2001), Blisniuk and Stern (2005), and Rowley and Garzione (2007).

We also collected modern water samples from modern wetlands and a Tsangpo River tributary near Zhongba ((N29° 39.754', E84° 10.056', 4 569 m, fig. 3, table A1). Water was collected from ponds, from which we collected modern gastropod samples (see section below), on the 18th of May and on the 26th of July, 2006. Water sample 180506-4 was collected with gastropod sample TSP16 and sample 180506-5 was collected with TSP18. Wetland ponds are < 100 m in diameter and < 0.5 m deep and are inset into both exhumed paleo-wetlands and modern dune fields. On the 26th of July we also collected water from the Tsangpo tributary. The river water collection location was within 10 km of the wetland water and gastropod collection sites for samples 260706-3, 180506-4 and TSP16 and, in the absence of alternative sources, is inferred to be the source water for the wetlands.

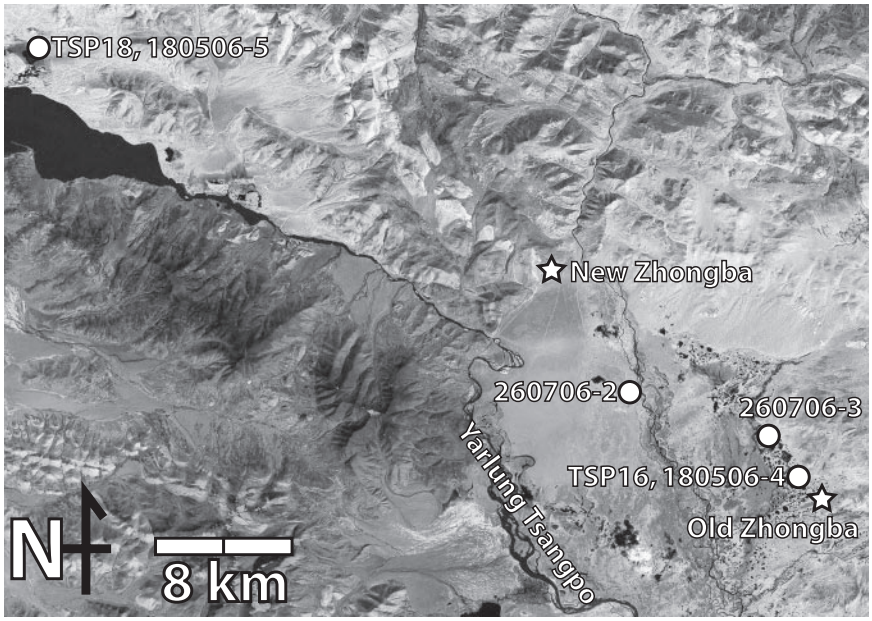

Fig. 3. Modern water and gastropod sample locations from the Zhongba area. Image from LandSat7.

Waters were analyzed for δD values using a dual inlet mass spectrometer (Delta-S, Thermo Finnegan, Bremen, Germany) equipped with an automated chromium reduction device (H-Device, Thermo Finnegan) for the generation of hydrogen gas using metallic chromium at 750°C. Water $\delta^{18}O$ values were measured on the same mass spectrometer using an automated CO_2-H_2O equilibration unit. Standardization is based on internal standards referenced to VSMOW and VSLAP. Precision is better than ± 0.08 permil for $\delta^{18}O$ and ±1 permil for δD.

Gastropods

We sampled fossil gastropods in two measured sections spanning the lower ~ 650 m of the Zhada Formation. No gastropod samples were found above ~ 650 m. Shell fragments and intact shells were collected from fluvial, marshy, and lacustrine intervals. We analyzed both homogenized gastropod shell material and micro-drilled gastropod shells to obtain seasonal information. To check for preservation of biogenic aragonite, 12 representative gastropod samples from fluvial, lacustrine and marshy intervals were powdered and analyzed using the University of Arizona's D8 Advance Bruker X-ray powder diffractometer.

We also collected gastropod shells from modern wetlands near Zhongba on the Tsangpo River (N29° 39.754', E84° 10.056', 4,569 m, fig. 3). Gastropod shells were collected from the shore of wetland ponds on the 18th of May, 2006. Gastropods were recently living and appeared to have died as the water table dropped. We analyzed one homogenized shell sample and microdrilled another at 0.3 mm increments.

We measured $\delta^{18}O$ and $\delta^{13}C$ values of shell material using an automated carbonate preparation device (KIEL-III) coupled to a gas-ratio mass spectrometer (Finnigan MAT 252). Powdered samples were reacted with dehydrated phosphoric acid under vacuum at 70°C. The isotope ratio measurement is calibrated based on repeated measurements of NBS-19 and NBS-18 and precision is ± 0.1 permil for $\delta^{18}O$ and ±0.06 permil for $\delta^{13}C$ (1σ).

Zhada Formation Plant Material

We analyzed 36 samples of organic matter from 29 stratigraphic intervals in two measured sections. Fossil plant material obtained from our sections is both fragmen-

tary and locally carbonized, but often preserves primary epidermal cell tissue. Much of this fossil plant material appears to be grass bladelets rather than leaves or twigs. Organic material was reacted with sulfurous acid in silver foil boats at least twice to remove carbonate material prior to drying at 60°C. We measured the $\delta^{13}C$ values of plant material on a continuous-flow gas-ratio mass spectrometer (Finnigan Delta PlusXL). Samples were combusted using an elemental analyzer (Costech) coupled to the mass spectrometer. Standardization is based on NBS-22 and USGS-24 for $\delta^{13}C$. Precision is better than $\pm$ 0.06 for $\delta^{13}C$ (1σ), based on repeated internal standards.

RESULTS

Age

We used several temporal anchors independent of magnetostratigraphy to constrain the magnetostratigraphic correlations. The first was the occurrence of *Hipparion* fossils at 310 m in our East Zhada measured section and at 240 m in our South Zhada measured section. Pilbeam and others (1996) placed the first appearance of *Hipparion* (the *Hipparion* datum) at 10.7 to 10.8 Ma in northern Pakistan. *Hipparion* radiated quickly (Woodburne and others, 1996; E. Lindsay, personal communication), thus the onset of sedimentation in Zhada Basin must be no earlier than 10.7 to 10.8 Ma. Additional Zhada fauna include *Hipparion zandaense*, *Nyctereutes*, and *Paleotragus microdon* (Zhang and others, 1981; Li and Li, 1990; X. Wang, personal communication). This biostratigraphic evidence constrains basin filling at Zhada to the late Miocene – Pliocene.

A shift in $\delta^{13}C_{pm}$ (plant material) values was observed in two of our sections (fig. 4). The $\delta^{13}C_{pm}$ values of plant organic matter are determined by the plant metabolic pathway. C_3 plants, mostly trees, shrubs and cool-growing-season grasses respire CO_2 with $\delta^{13}C$ values that average -27 $\pm$ 6 permil globally. C_4 plants, including some shrubs, but primarily warm-growing-season grasses, respire CO_2 with $\delta^{13}C$ that average -13 ± 3 permil globally (Ehleringer and others, 1991). Quade and others (1995, 1989) and France-Lanord and Derry (1994) showed a marked shift in $\delta^{13}C_{pm}$ values in paleosol carbonate and plant material in the Indian subcontinent at $\sim 7 \pm 1$ Ma. They attributed this shift to a change from C_3 to C_4 dominated plants. In far western Nepal, ~300 km SSE of Zhada Basin, Ojha and others (2000) place the C_3 – C_4 transition at 7 Ma. Garzione and others (2000a) used this same shift in the Thakkhola graben in the southern Tibetan Plateau (500 km SE of Zhada Basin) as an anchor for their magnetostratigraphic correlation. Finally, the presence of C_4 plants in the diet of fossil

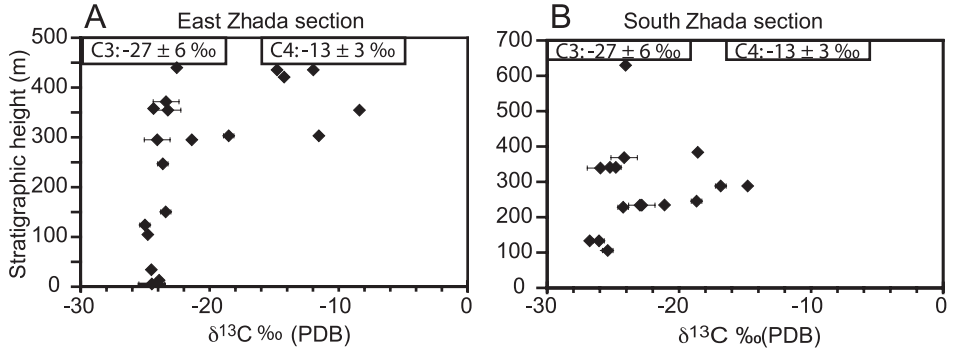

Fig. 4. $\delta^{13}C$ of vascular organic material versus stratigraphic level for the South Zhada and East Zhada measured sections. In both sections we see the introduction of C_4 plants ($\delta^{13}C$ values > -16‰) at 250 – 300 m. The shift in $\delta^{13}C$ values, from uniformly negative to a mixture of more and less negative values at 250 – 300 m, is seen in the northern Indian sub-continent and southern Tibetan Plateau and is associated with a change in biomass from C3 dominated to a mix of C3 and C4 or C4 dominated biomass at ~ 7 Ma.

herbivores was used as independent confirmation of the post 7 to 8 Ma age of the fossils in Gyirong Basin (Wang and others, 2006).

We first correlated our South Zhada (SZ) and Southeast Zhada (SEZ) magnetostratigraphic sections using the capping geomorphic surface as a datum (fig. 2A). This surface is correlative across the basin and marks the maximum extent of sedimentation prior to incision and exhumation by the Sutlej River. This approach assumes that the geomorphic surface is isochron. The validity of this assumption is based on the interpretation of the geomorphic surface as a depositional surface that extended across the basin just prior to incision and abandonment. The assumption is also based on the gross similarities between the upper portions of the South Zhada and Southeast Zhada magnetostratigraphic (and lithologic) sections. Working downward from the datum, the longest normal and reversed polarity intervals were correlated between the two sections. A composite magnetostratigraphic column was then created that incorporated both long polarity intervals and also the shorter polarity intervals from both sections (fig. 2B). This approach assumes that whereas the shorter polarity intervals may have been missed in one or the other section, the longer polarity intervals were not. Combining data from both magnetostratigraphic sections produces a composite magnetostratigraphic section that is more detailed than either of the individual sections (fig. 2B).

The mammal megafaunal fossil anchor described above and the number of polarity chrons in the composite section indicate that sedimentation extended from the late Miocene to the Pliocene or Pleistocene. Within these constraints we correlated the composite section with the Global Polarity Time Scale (GPTS) of Cande and Kent (1995). Intervals P+ through T+ likely correlate with either chron 2An or 3n (figs. 2C, 2E, and 2G). We favor the correlation in figure 2E for several reasons. This correlation (1) accounts for all of the normal and reversed intervals, (2) places the C_3 – C_4 transition at $\sim$ 7 Ma, which is consistent with its age elsewhere, and (3) yields relatively constant and reasonable sedimentation rates. The alternative correlations have several drawbacks. The correlation in figure 2C means that the upper geomorphic surface is $\sim$ 3 Myr old and yet shows no evidence for significant erosion. The correlation of chrons 3r – 4n is equally problematic in correlation G as evidenced by the large excursions in the sediment accumulation rates (fig. 2H). With those considerations, the base of the composite section most reasonably correlates to chron 4Ar.1 and the top of the section to chron 1n (fig. 2E). This corresponds to an absolute age interval of $<$ 1 to 9.2 Ma (Cande and Kent, 1995). While the correlation in figure 2E is favored, both E and C place the onset of sedimentation at $\sim$ 9.2 Ma. The onset of sedimentation in both correlations E and C is consistent with an independent magnetostratigraphy study conducted by Wang and others (2008a). They differ significantly only in the upper portion, which is not the focus of this paper.

Modern Water

Modern $\delta^{18}O_{sw}$ (surface water) values range from -17.9 to -11.9 permil, and δD_{sw} values from -137 to -86 permil (VSMOW, fig. 5, table A1) for water from the Zhada Basin. The lowest values coincide with small springs draining catchments in the Himalaya to the south of Zhada Basin. The average $\delta^{18}O_{sw}$ value of the water coming from the Ayi Shan, to the north of Zhada Basin (fig. 1B), is slightly higher than for water coming from the Himalaya (-14.1 and -15.3‰, respectively). The average $\delta^{18}O_{sw}$ value of water from the Sutlej River main stem (-15.1‰) reflects input from both of these sources. The modern $\delta^{18}O_{sw}$ values for water from the Zhongba area range from -18.9 to -3.9 permil and δD_{sw} values range from -140 to -86 permil (VSMOW, fig. 5, table A1).

Gastropods

XRD analysis from 11 of 12 samples yielded only aragonite peaks (fig. A3). One sample was too small to yield results and was removed from further consideration. The

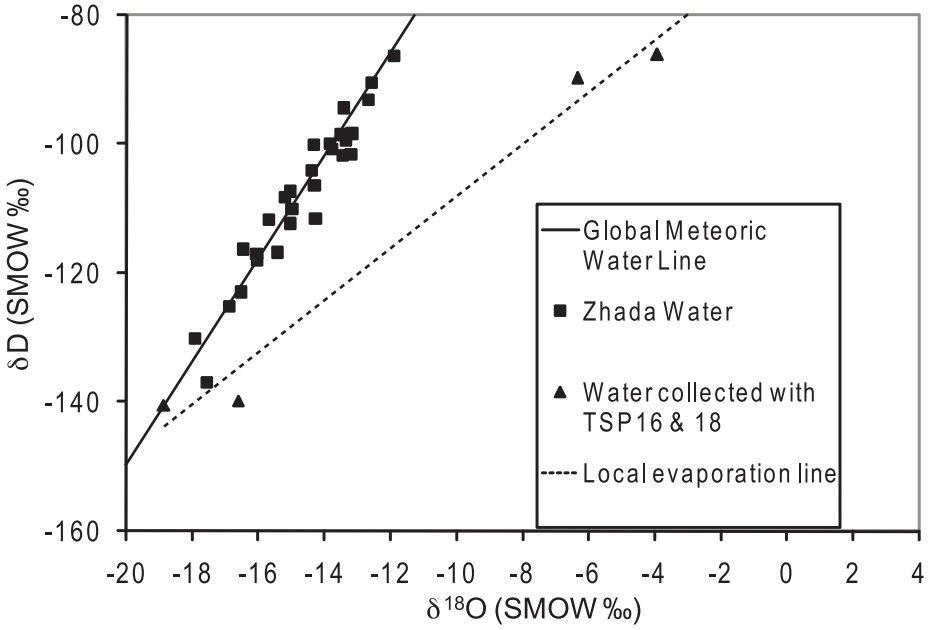

Fig. 5. Stable isotope composition of modern water from the Zhada Basin and Zhongba area plotted against the Global Meteoric Water Line. The dotted line is a mixing line between evaporated wetland samples and an unevaporated fluvial sample from Zhongba.

$\delta^{18}O_{cc}$ (carbonate) values of samples that we analyzed using X-ray diffraction ranged from −20.3 to +0.2 permil (VPDB).

$\delta^{13}C_{cc}$ (carbonate) values of gastropods range from −13.8 to +7.5 permil (table A2). Consideration of the data as a whole shows clear covariance between $\delta^{13}C_{cc}$ and $\delta^{18}O_{cc}$ values (R^2 value of 0.61 for the South Zhada section and 0.62 for the East Zhada section; fig. 6). Dividing the data by lithofacies reveals a more complex pattern (fig. 6). $\delta^{13}C_{cc}$ values of samples from fluvial intervals range from −13.8 to −2.6 permil and show almost no covariance (fig. 6). $\delta^{13}C_{cc}$ values of samples from supralittoral/marshy intervals range from −13.8 to +7.5 permil and display significantly more covariance (fig. 6). Samples from littoral intervals yield $\delta^{13}C_{cc}$ values of −3.8 to +3.0 permil and show moderate covariance (fig. 6). Finally, samples from profundal lacustrine inter-

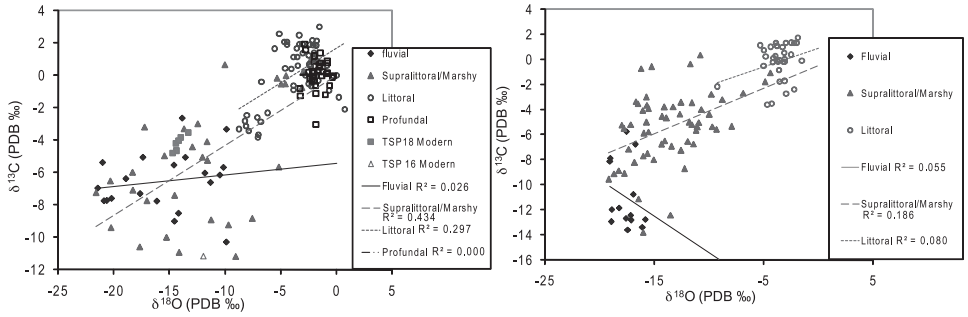

Fig. 6. Oxygen and carbon isotope covariance for gastropods from the Zhada formation showing covariance patterns for lithofacies assemblages. Correlation coefficients for the entire data sets are 0.65 and 0.62 for South Zhada and East Zhada respectively. Also shown in (A) are $\delta^{18}O_{cc}$ and $\delta^{13}C_{cc}$ values for modern gastropods from the Zhongba wetlands

vals, which only occur in the South Zhada section, yield $\delta^{13}C_{cc}$ values of −3.0 to +1.9 permil and show no covariance (fig. 6).

$\delta^{18}O_{cc}$ values of gastropods from fluvial intervals range from −21.4 to −9.9 permil (VPDB); from supralittoral/marshy intervals between −21.6 to −1.8 permil; from littoral intervals, −9.3 to +0.7 permil and from profundal intervals, −3.2 to +0.3 permil (table A2, fig. 7). Finally, microdrilled samples show a range of $\delta^{18}O_{cc}$ values, typically ~ 3 permil but up to 10.9 permil, from a single sample (fig. 8). All the snails are aquatic.

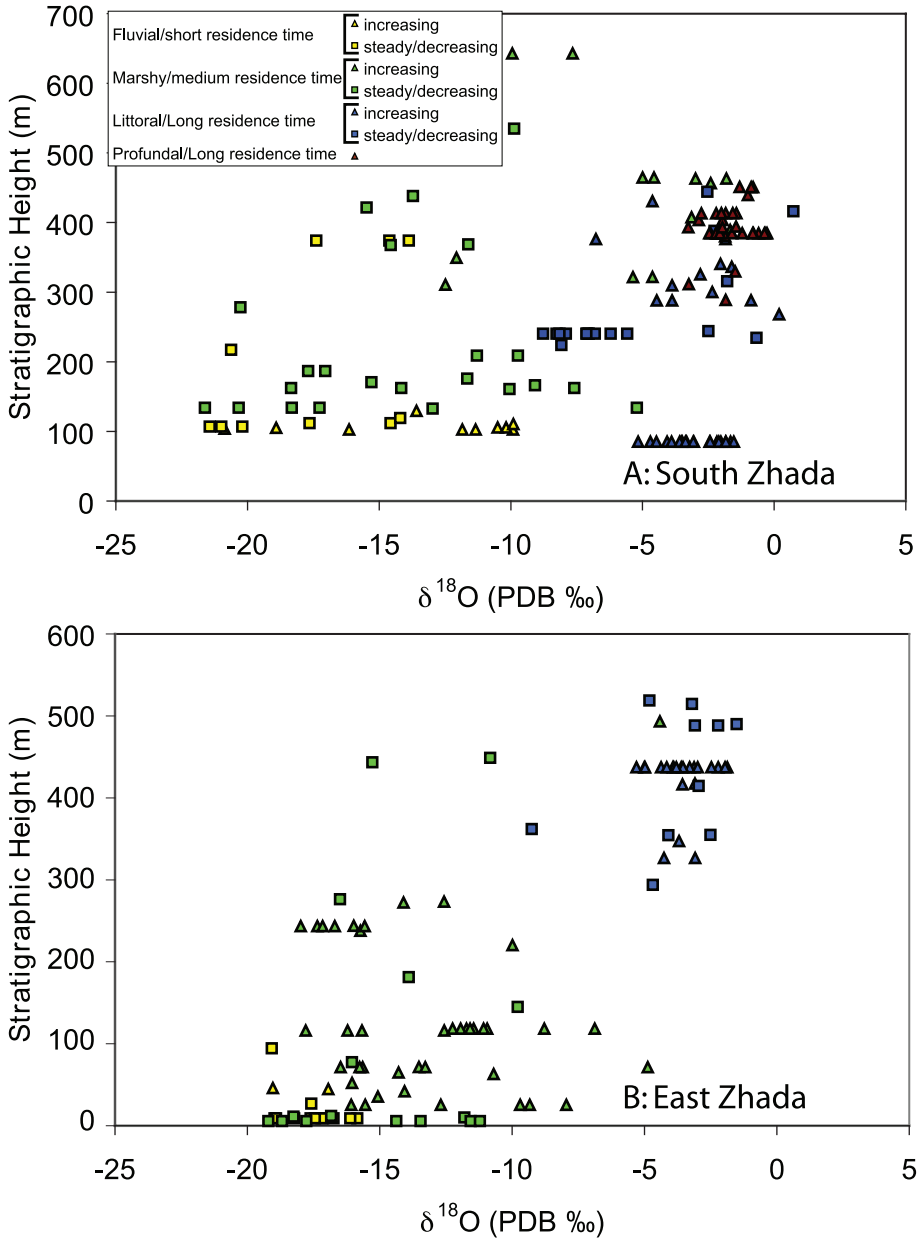

Fig. 7. $\delta^{18}O$ (VPDB ‰) and stratigraphic height for Miocene – Pleistocene gastropods from (A) South Zhada and (B) East Zhada subdivided by lithofacies assemblages.

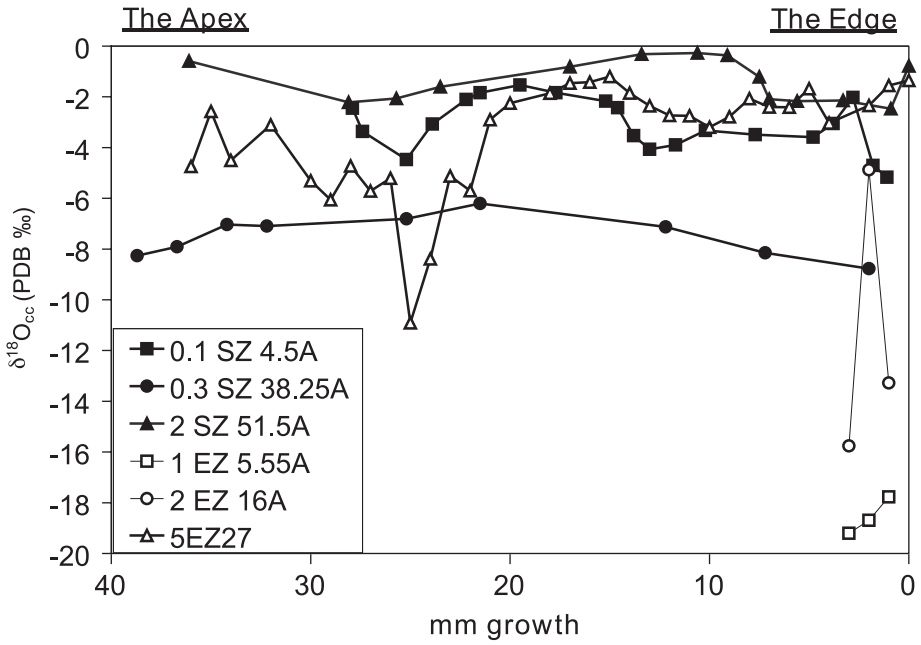

Fig. 8. $\delta^{18}O$ (VPDB ‰) and mm growth from seasonally sampled Miocene – Pleistocene gastropods from Zhada Basin. Typical seasonal variations are between 2 – 3‰. Sample 2EZ16A is from a marshy interval and shows evidence of a drying episode. Sample 5EZ27 is from a deltaic sequence and shows evidence of a freshening episode.

$\delta^{18}O_{cc}$ values of modern gastropods from Zhongba range from −12.0 to −14.7 permil and (VPDB) $\delta^{13}C_{cc}$ values range from −3.6 to −11.2 permil (VPDB). The two samples do not show an obvious covariant trend, though sample TSP18 may show internal covariance (fig. 6).

Zhada Formation Plant Material

$\delta^{13}C_{pm}$ values range from −23.4 to −26.8 permil (VPDB) in the lower 250 to 300 m of both sampled sections, and increase to as high as −8.4 permil (VPDB, table A3, fig. 4) above 300 m.

APPLICATION TO PALEOALTIMETRY

Calculation of Miocene $\delta^{18}O_{sw}$ and Related Constraints and Corrections

Source, pathway and amount effect constraints.—Applying the modern $\delta^{18}O$ versus elevation lapse rates to the Miocene requires accounting for potential climate change in the intervening time. Currently, the Indian subcontinent's summer monsoon derives its water vapor from the Arabian Sea and Indian Ocean. Source region temperatures influence the $\delta^{18}O$ values of high-elevation carbonates in two ways: 1) sea surface temperatures effect the $\delta^{18}O$ value of source region water vapor (Jouzel and others, 1997; Blisniuk and Stern, 2005), and 2) low-elevation temperatures effect the $\delta^{18}O$ versus elevation lapse rate (Rowley and others, 2001; Rowley and Garzione, 2007). Modern mean annual temperature (MAT) for the low-elevation Himalayan foreland is 25 °C or 27 to 28 °C for coastal IAEA/WMO GNIP stations (Mumbai and Calicut; IAEA/WMO, 2007). Current MAT is close to the MAT of 26.5 °C calculated from Miocene soil carbonate nodules in western Nepal (Quade and others, 1995), as well as MAT estimates based on fossil flora assemblages (for example, Awashi and Prasad,

1989; Sarkar, 1989). Lower low-elevation temperatures would elevate the $\delta^{18}O$ versus elevation lapse rate, and hence reconstructed paleoelevations would overestimate paleoelevation. As noted above, neither regional nor global late temperature estimates indicate an increase in temperature between the late Miocene and the modern (Zachos and others, 2001). Miocene sea surface temperatures have typically been thought to be ~ 10° C cooler than the modern (Kennett, 1985; Savin and others, 1985; Williams and others, 2005). Lower Miocene sea-surface temperatures would result in low-elevation water vapor with higher $\delta^{18}O$ values hence reconstructed paleoelevations would underestimate the actual paleoelevation. However, there is debate whether measured $\delta^{18}O$ values represent sea-surface temperatures or the bottom temperature during early diagenesis (for a brief summary see Pearson and others, 2002; Zachos and others, 2002). This raises the possibility that Miocene Indian Ocean sea surface temperatures were comparable to the modern (Stewart and others, 2004; Williams and others, 2005). Additionally, average paleosol $\delta^{18}O_{cc}$ values from Neogene deposits at low elevation in the northern Indian sub-continent show no change post-8 Ma (Quade and others, 1995). Araguas-Araguas and others (1998, fig. 1) indicate that moisture up to and just north of the crest of the Himalaya is dominated by moisture from the Indian summer monsoon. The Zhada basin is located just north of the crest of the Himalaya and all drainages on the southern side of the basin are sourced by glaciers that originate at the foot of high Himalayan peaks to the south. The implication is that at least half the water in the basin is coming from the Himalaya. According to Tian and others (2001), rainfall with high deuterium-excess (d-excess) values in the Himalaya and just north of the Himalaya is derived from the Indian summer monsoon. Water from the Zhada basin has d-excess values of between 3 and 15 (mean: 10) which is consistent with derivation from the Indian summer monsoon. Finally, the Zhada basin is located far to the west of the range of penetration of Pacific moisture onto the Tibetan Plateau (Araguas-Araguas and others, 1998, fig. 1).

Paleosols from northern India would have experienced the same climate changes and changes in source water $\delta^{18}O$ values as the Zhada samples, since northern India is dominated by the same monsoon climate system (Araguas-Araguas and others, 1998; Dettman and others, 2001; Tian and others, 2001). As no significant change in MAT or $\delta^{18}O_{cc}$ values is evident from the low-elevation late Miocene records, we apply current climatic conditions in reconstructing $\delta^{18}O_{psw}$ (paleo-surface water) values (Quade and others, 1995). Since the monsoon seems to have been established by at least 10.7 Ma (Dettman and others, 2001), the same source and pathway applies for Miocene Zhada meteoric water as for modern Zhada meteoric water. This suggests that we can use the modern $\delta^{18}O$ versus elevation relationships, as measured by Garzione and others (2000b) and modeled by Rowley and others (2001), to understand the ancient record.

Shell preservation.—We are confident that gastropod samples are unaffected by diagenesis and retain their original $\delta^{18}O_{cc}$ values for the following three reasons: (1) all of the samples which returned usable X-ray diffraction results (11 of 12) were aragonite (see Appendix fig. A3), and none showed evidence of recrystallization; (2) the samples are visually pristine, retaining a pearly luster in the interior and obvious growth bands; and (3) samples which we microdrilled showed seasonal variation (fig. 8). Such internal variation would not be expected if the samples were overprinted by a regional $\delta^{18}O_{sw}$ value during diagenesis. The results from this representative sampling can be confidently applied across the basin because the sediments were never buried below ~ 800 m and so are not subject to regional metamorphism or hydrothermal alteration.

Calculation of Miocene $\delta^{18}O_{psw}$.—$\delta^{18}O_{psw}$ values were reconstructed from $\delta^{18}O_{ar}$ values using:

$$\delta^{18}O_{psw}\,(\mathrm{VSMOW}) = [(1000 + \delta^{18}O_{cc}\,(\mathrm{VSMOW}))/\{\exp\{[2.559 * 10^6 * T^{-2} + 0.715]/1000\}\}] - 1000 \quad (1)$$

(Dettman and others, 1999; modified from Grossman and Ku, 1986) where T (in K) is the temperature of CO_3 precipitation. We used the modern temperature to constrain the temperature of aragonite precipitation (see section *Source, pathway and amount effect constraints*). The nearest weather station for which there are long term records is at Shiquanhe (32.5°N, 80.083°E, 4280 m) (NCDC, 2007). MAT at Shiquanhe for the period between 1969 and 1990 is 0°C. Assuming that gastropods grow dominantly during the warmer months, we calculated the average temperature for the months of April – October (months when $T_{average} > 0°C$) and set T = 7°C. Warmer temperatures produce higher $\delta^{18}O_{psw}$ values, thus lowering paleoelevation estimates. Intrashell variation of ± 1.5 permil corresponds to a seasonal variation of ± 7°C and that uncertainty is applied to all samples (fig. 9).

Comparison with Models

Effect of paleotemperature.—One possible explanation for the extremely low $\delta^{18}O_{cc}$ values of gastropod aragonite (fig. 7) is that it was precipitated in warm water. If we assume no change in $\delta^{18}O_{sw}$ values of water in the Zhada region [that is, that the most negative $\delta^{18}O_{sw}$ value of modern Zhada water (-17.9 ‰ VSMOW) is representative of the water in which late Miocene gastropods lived], we can use the fractionation factor between that water and the gastropod aragonite $\delta^{18}O_{cc}$ value (-21.6‰ VPDB) to calculate the temperature of precipitation. However, this exercise yields an unrealistic temperature of aragonite precipitation of 41° C. Thus, the temperature of aragonite precipitation alone cannot explain the extremely negative $\delta^{18}O_{cc}$ values.

Modeling changes in lapse rate.—By changing input parameters for thermodynamically based $\delta^{18}O$ versus elevation models (Rowley and others, 2001; Rowley and Garzione, 2007) we can evaluate the effect of 1) changes in monsoon intensity on the $\delta^{18}O$ versus elevation lapse rate and 2) changes in low-elevation temperature. We first looked at the effect of increasing monsoon intensity on the $\delta^{18}O$ versus elevation lapse rate. We calibrated the model by finding the low-elevation temperature that produces a lapse rate that is consistent with the most negative modern Zhada water (−17.9‰ VSMOW with a mean catchment elevation of 5,419 m). This yielded a low elevation temperature of 297.5 K. While maintaining the low elevation temperature at 297.5 K, we artificially decreased the saturation vapor pressure of the system to find a model lapse rate that places the reconstructed Miocene water value at 5,419 m. Decreasing the saturation vapor pressure artificially forces increased precipitation, and thus decreased $\delta^{18}O_{sw}$ values, at lower elevations. The best fit was found when the saturation vapor pressure was decreased by 30 percent. However, there is no evidence from lowland $\delta^{18}O_{cc}$ records of changes in $\delta^{18}O_{sw}$ values consistent with a change in precipitation amount of this magnitude (Quade and others, 1995; Dettman and others, 2001).

We also considered changes in low elevation temperature. Assuming that the $\delta^{18}O$ value of the reconstructed Miocene – Pleistocene water from Zhada Basin (−24.5‰ VSMOW, fig. 9) is accurate, we changed the low elevation temperature to find a model lapse rate which places that $\delta^{18}O$ value at 5,419 m. A match was found at a low elevation temperature of 293 K, a decrease of 4.5 °C from the modern. This decrease in temperature should show up in the low-elevation $\delta^{18}O_{cc}$ and paleobotanical records and in the climate record in Zhada Basin. However, as noted above, the low-elevation $\delta^{18}O_{cc}$ and paleobotanical records post-8 Ma are consistent with the modern. Moreover, global climate is thought to have cooled between the Miocene and the present, not warmed as would be required by this scenario (for example, Zachos and others, 2001).

Evaporation vs. Outflow

Comparing $\delta^{18}O_{cc}$ values from fluvial and lacustrine gastropods allows reconstruction of local climate conditions if we can estimate outflow from the basin. We used

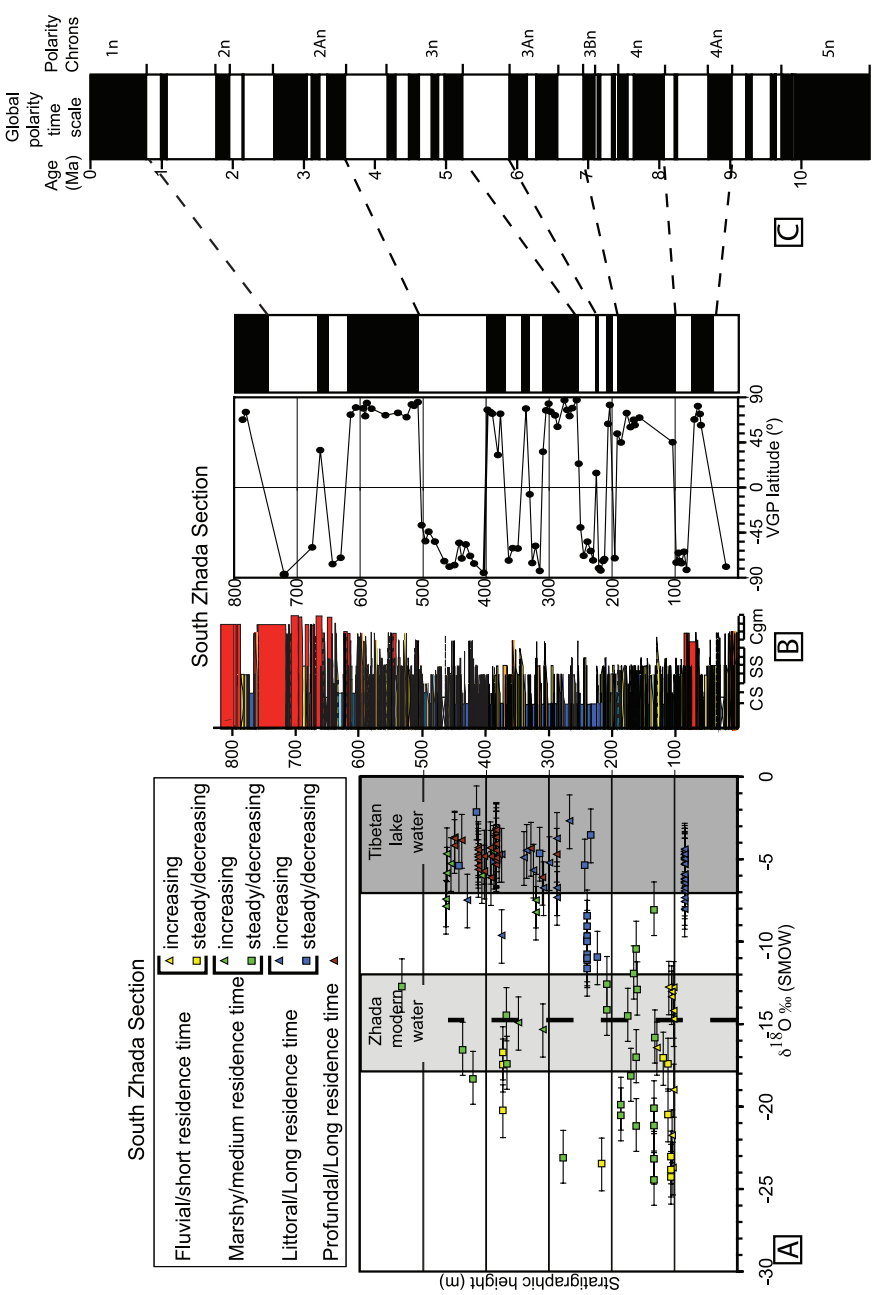

Fig. 9. (A) Calculated $\delta^{18}O_{psw}$ values from gastropods from the South Zhada measured section. Error bars represent an uncertainty of ± 7°C due to possible seasonal variation in the temperature of carbonate precipitation. The range of modern fluvial or stream water (−17.9 to −11.9 ‰: light gray box) and mean value for modern water (−14.8‰: dashed vertical line) as well as the range of values obtained from modern Tibetan lakes (+1.7 to −7.1‰: dark gray box) are shown for comparison. $\delta^{18}O_{psw}$ values from gastropods from fluvial intervals are at least as negative as the corrected modern, reflecting elevations at least as high as the modern. $\delta^{18}O_{psw}$ values from gastropods from lacustrine intervals are at least as positive as those from modern lakes, reflecting an environment that, like the modern, was arid. (B) South Zhada measured stratigraphic section. (C) Site-mean virtual geomagnetic pole (VGP) latitude for the South Zhada section plotted against stratigraphic level and correlated with the global polarity timescale of Cande and Kent (1995). Positive VGP latitudes indicate normal polarity shown by black intervals and negative VGP latitudes indicate reversed polarity shown by white intervals.

−21.6 permil (VPDB) as our inflow value, based on the $\delta^{18}O_{cc}$ values of the fluvial fossil mollusks. The range of $\delta^{18}O_{cc}$ values of −3.3 permil and −0.4 permil (VPDB) for lacustrine mollusks corresponds to $\delta^{18}O_{sw}$ values of −6.2 and −3.3 (VSMOW), respectively, (assuming a temperature of precipitation of 7 °C). These paleo-lake water $\delta^{18}O$ values are within the range of −7.1 to +1.7 permil (VSMOW) observed in modern lakes on the Tibetan Plateau (Gasse and others, 1991; Fontes and others, 1996; Quade, unpublished data). The range of total enrichment values ($\varepsilon_{w\text{-}v}$ = 18.7 – 21.7) was calculated based on our inflow $\delta^{18}O_{cc}$ value and the range of lacustrine $\delta^{18}O_{cc}$ values.

We compared the calculated Miocene enrichment values to modeled modern isotopic enrichment values for relative humidity values between 0 and 70 percent and temperatures between 0 and 10 °C. The modern average relative humidity is 30 percent, reaching a maximum of 50 percent during the monsoon. The modern MAT is 0 °C, average temperature between April and October is 7 °C, maximum monthly temperature is 14 °C and the maximum temperature between 1961 and 1990 is 21 °C.

The total isotopic enrichment, $\varepsilon_{w\text{-}v}$, is a function of both the equilibrium water – boundary layer enrichment ($\varepsilon_{w\text{-}bl}$) and a kinematic enrichment ($\varepsilon_{bl\text{-}v}$). We calculated the kinetic enrichment during evaporation using the equation:

$$\varepsilon_{bl\text{-}v} = 14.2\ (1\text{-rh}), \tag{2}$$

where $\varepsilon_{bl\text{-}v}$ is the enrichment in permil between a saturated boundary layer above the water surface and a well-mixed vapor column and rh is the relative humidity fraction (Gonfiantini, 1986). The $\delta^{18}O$ value of evaporation was calculated using a simple mixing equation such that

$$\delta^{18}O_{evap} = (\delta^{18}O_{inflow} - f * \delta^{18}O_{lake})/(1 - f)) \tag{3}$$

where f is the outflow fraction. We assume that f = 0.

The equilibrium enrichment was calculated using:

$$1000\ln\alpha(\delta^{18}O_{w\text{-}bl}) = 1.137(10^6/T^2) - 0.4156(10^3/T) - 2.0667 \tag{4}$$

(Majoube, 1971) where T is temperature in Celsius.

One source of uncertainty is whether or not the basin was closed. Increasing the outflow fraction would result in increasing the total (outflow + evaporative) enrichment. The $\delta^{18}O_{cc}$ record in closed-basin gastropod shells could easily be identical to $\delta^{18}O_{cc}$ values for open-lake gastropod shells if conditions were cooler or drier. Hence, we are unable to determine whether or not outflow has occurred from the $\delta^{18}O_{cc}$ values. However, the occurrence of mudcracks and bedded gypsum in the sedimentary sections, in addition to the covariance between $\delta^{18}O_{cc}$ and $\delta^{13}C_{cc}$ values, suggests that Zhada Basin was at least periodically, if not continually, closed during lacustrine sedimentation.

The results of modeling the relative humidity, isotopic enrichment, and temperature confirm that there is a limited range of reasonable values for all of these variables and that range is consistent with the modern climate in the area (fig. 10).

Temperature of Modern Gastropod Shell Precipitation

The $\delta^{18}O_{cc}$ values of modern gastropods from near Zhongba, coupled with the $\delta^{18}O_{sw}$ values of water in which those gastropods lived, allows calculation of a fractionation factor and hence a temperature of aragonite precipitation. In the following discussion "pre-monsoon wetland water" refers to water with $\delta^{18}O_{sw}$ values of between −3.9 and −6.3 permil (VSMOW) and "monsoon wetland water" refers to water with $\delta^{18}O_{sw}$ values of −16.6 permil (VSMOW). We first assumed that the gastropods precipitated their shells in equilibrium with the pre-monsoon wetland water they were near on the date of collection (18th May, 2006). However, this results in

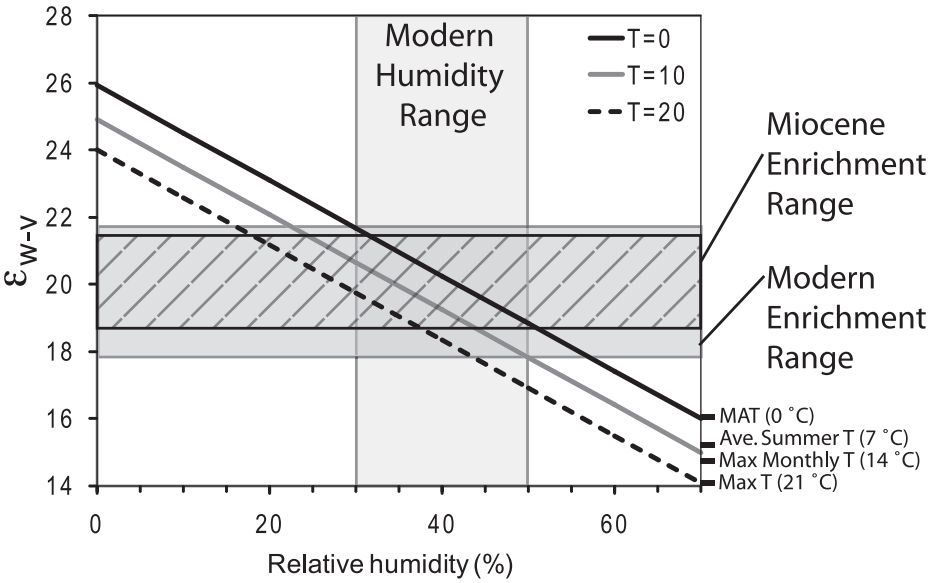

Fig. 10. Modeled enrichment values (horizontal gray box) for the modern relative humidity range (vertical gray box) and temperatures between 0 and 10 °C compared with Miocene enrichment (diagonally ruled box). Miocene enrichment (21.7 to 18.7‰) is based on the difference in $\delta^{18}O$ between fluvial and lacustrine gastropods. Also shown are the mean annual temperature (0 °C), average temperature from April – October (7 °C), maximum mean month temperature (14 °C) and absolute maximum temperature (21 °C) for 1961 – 1990 at Shiquanhe weather station. Calculated Miocene enrichment values overlap modeled modern enrichment values, indicating that the climate in the Miocene was cold and arid, very similar to the modern.

unreasonably high temperatures of aragonite precipitation (fig. A4). Alternatively, assuming that the gastropods precipitated their shells in equilibrium with monsoon wetland water (sample 260706-3) results in temperatures between ~ 0 to 12 °C (fig. A4). These temperatures are between MAT and the maximum average monthly temperature for the period 1961 to 1990 as recorded by the Shiquanhe weather station.

We can calculate the relative contribution of oxygen from pre-monsoon and monsoon wetland water to shell aragonite if we assume a range of temperature of aragonite precipitation of 0 to 12 °C. We used a simple mixing ratio between aragonite precipitated in equilibrium with monsoon and pre-monsoon wetland waters at 0 and 12 °C. Applying this calculation to sample 180506-4 shows that shell $\delta^{18}O_{cc}$ values of −12 permil (VPDB) require that the shells are 100 percent aragonite precipitated in equilibrium with monsoon wetland water at 0 °C or ~ 70 percent aragonite precipitated in equilibrium with monsoon wetland water at 12° (fig. 11). A similar calculation for sample 180506-5 (average $\delta^{18}O_{cc}$ value ~ −14‰ VPDB) shows that if the temperature was 0 °C the shell must have been precipitated in water with $\delta^{18}O_{sw}$ values more negative than observed monsoon wetland water or, if the temperature was 12 °C, the aragonite was precipitated in equilibrium with 100 percent observed monsoon wetland water (fig. 11).

Paleoelevation models.—We compared the most negative $\delta^{18}O_{sw}$ and reconstructed $\delta^{18}O_{psw}$ values to $\Delta\delta^{18}O_{sw}$ versus elevation relationships based on both a simple Rayleigh fractionation model (Rowley and others, 2001; Rowley and Garzione, 2007) and an empirical data set (Garzione and others, 2000b). In calculating $\Delta\delta^{18}O_{sw}$, we used the modern, low-elevation $\delta^{18}O_{mw}$ value for New Delhi of −5.8 permil (VSMOW, Rozanski and others, 1993) and a Miocene low-elevation $\delta^{18}O_{cc}$ value of −6.0 permil

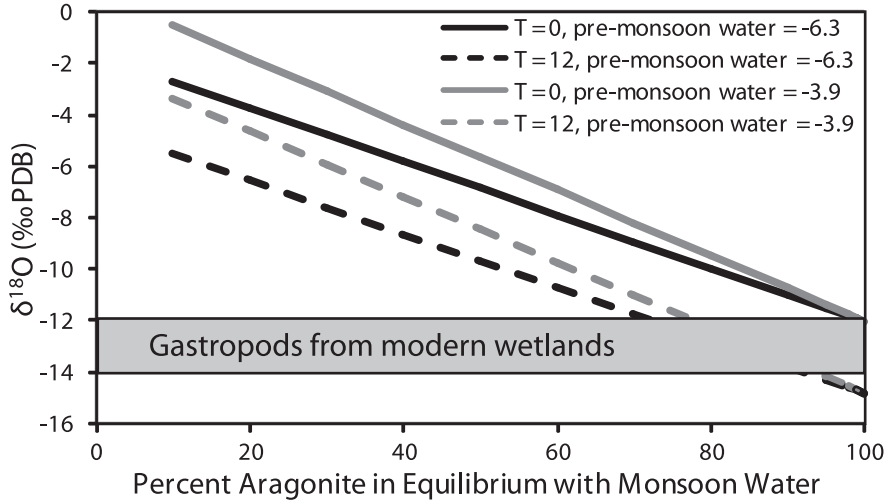

Fig. 11. Modeled percent of modern aragonite in equilibrium with monsoon wetland waters given various temperature and pre-monsoon wetland water $\delta^{18}O_{sw}$ values. The range of $\delta^{18}O_{cc}$ values of gastropods from modern wetlands along the Tsangpo River are shown in the horizontal gray shaded box.

(VSMOW) from paleosols from the Siwalik Group of Pakistan and Nepal (Quade and others, 1995; Dettman and others, 2001). Uncertainties in our $\Delta\delta^{18}O_{psw}$ value derive from a ± 0.5 permil uncertainty due to variation in the most negative values of $\delta^{18}O_{cc}$ in Miocene low-elevation paleosol carbonates between western Nepal and Pakistan (Quade and others, 1995), and ± 1.5 permil uncertainty due to seasonal changes in the temperature of aragonite precipitation (see section *Calculation of Miocene* $\delta^{18}O_{psw}$).

Additional uncertainty in paleoelevation estimates potentially arises from variability in the low-elevation temperature or humidity (Rowley and others, 2001; Rowley and Garzione, 2007). Modern surface water sampled in this study integrates multiple glacial sources and groundwater. Hence these samples do not represent a single precipitation event but rather a temporal average. Variability in modern samples that are derived from the same sources and are collected at the same elevation (see for example fig. 12), interpreted in terms of low-elevation temperature or humidity would lead to the conclusion that temporally averaged low-elevation temperature or humidity had varied dramatically. As this degree of variability in low-elevation parameters is not observed currently, we conclude that this approach incorrectly attributes variability causation. Hence, in our calculation of paleoelevation we use only the variability inherent in the reconstructed water $\Delta\delta^{18}O$.

The modern water samples from the Zhada region fall above the $\Delta\delta^{18}O_{sw}$ versus elevation curves based on both Rayleigh fractionation [with an initial, low-elevation temperature (T_i) = 295 K, and initial relative humidity (rh) = 0.8] and empirical data from Nepal (fig. 12). The implication is that a calculated paleoelevation based on either of these curves will be a minimum. $\Delta\delta^{18}O_{sw}$ values of modern water samples fall between a variation of the Rayleigh fractionation model with T_i = 303 K and rh = 0.8, and the models described above. A low elevation T_i = 300 K and rh = 0.8 is consistent with modern, coastal MAT in the Indian subcontinent. The modified Rayleigh fractionation model yields a best-fit polynomial of

$$z = -0.0014\,(\Delta\delta^{18}O)^4 - 0.488(\Delta\delta^{18}O)^3 - 30.88(\Delta\delta^{18}O)^2 - 814.19(\Delta\delta^{18}O), \quad (5)$$

where z is elevation in meters. A low-elevation temperature T_i = 303K and rh = 0.8 most closely matches the $\Delta\delta^{18}O_{sw}$ versus elevation relationship defined by the maxi-

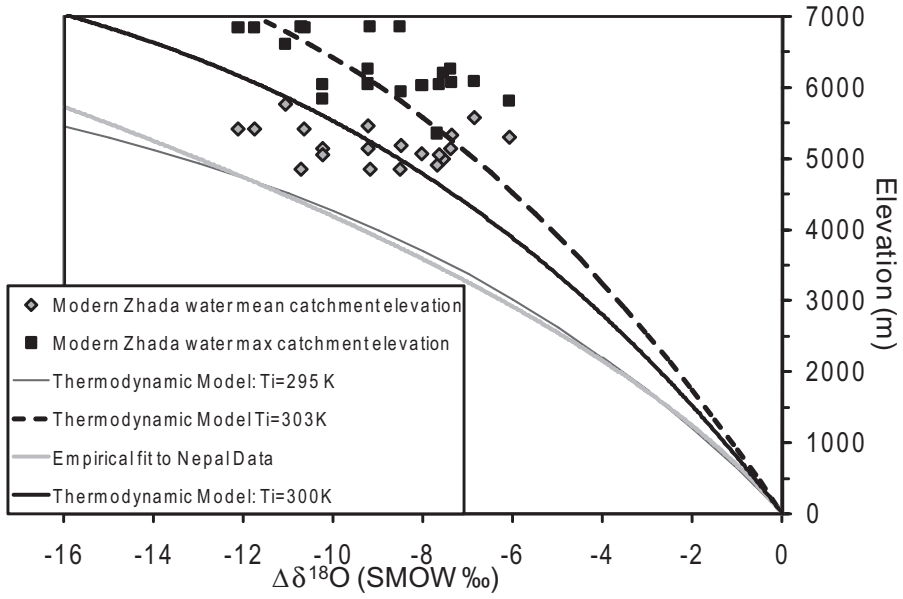

Fig. 12. $\Delta\delta^{18}O$ (VSMOW ‰) of modern water from the Zhada Basin and the mean and maximum catchment elevation for water samples. $\Delta\delta^{18}O$ is calculated assuming a low-elevation $\delta^{18}O$ value for New Delhi of −5.8 ‰. Also shown are thermodynamically based lapse rate models [based on work by Rowley and others (2001) and Rowley and Garzione (2007)] with low-elevation temperature of 303K (dashed line), 300 K (black line), and 295 K (thin black line) and an empirical lapse rate (from Garzione and others, 2000b, light gray line).

mum catchment elevation of the Zhada water samples. This relationship yields a best-fit polynomial of

$$z = 0.011(\Delta\delta^{18}O)^4 + 0.041(\Delta\delta^{18}O)^3 - 29.22(\Delta\delta^{18}O)^2 - 927(\Delta\delta^{18}O). \quad (6)$$

We applied the Rayleigh fractionation models with $T_i = 295$ K and $T_i = 300$ K and the empirically based model to our data in order to compare the elevations predicted by $\Delta\delta^{18}O_{sw}$ values of modern water with those predicted by the $\Delta\delta^{18}O_{psw}$ values of our reconstructed Miocene – Pleistocene water. Whereas the absolute elevations of our modern water samples do not match those predicted by several of the models (fig. 12), we are interested – at this point – in the difference in elevation predicted by the models.

In all three of the models there is a difference in predicted elevations between our most negative $\delta^{18}O_{psw}$ value and our most negative $\delta^{18}O_{sw}$ value that is greater than the uncertainty associated with those data points (fig. 13). The Rayleigh fractionation model with $T_i = 295$ K yields a minimum predicted elevation from $\Delta\delta^{18}O_{psw}$ values (mean elevation – uncertainty) of 5.6 km and a predicted elevation for the modern water sample of 4.8 km. This adds up to an elevation decrease of *at least* 0.8 km since the late Miocene. Doing the same calculation for either the Rayleigh fractionation model with $T_i = 300$ K or the empirically based curve results in a minimum elevation decrease of at least 1 km or 1.2 km, respectively. More realistically, comparing the mean values for each of the $\Delta\delta^{18}O_{sw}$ versus elevation curves yields elevation decreases of 1.0 (± 0.2) km, 1.2 (± 0.2) km and 1.5 (+ 0.3 - 0.4) km for the Rayleigh fractionation models with $T_i = 295$ K and $T_i = 300$ K and the empirically based curve, respectively. Although the models are inconsistent with regards to absolute elevation, yielding an inter-model range of elevations (z) of 1.4 km for modern water and 1.6 km

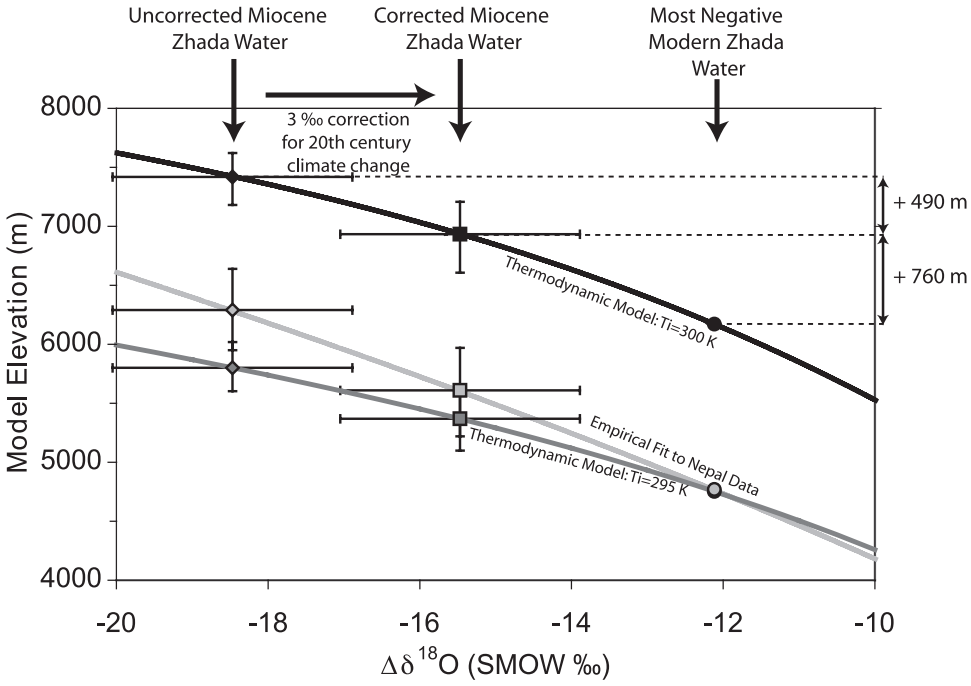

Fig. 13. $\Delta\delta^{18}O$ (VSMOW ‰) values for the most negative modern Zhada water samples and most negative reconstructed Miocene – Pleistocene water and modeled elevation for thermodynamically based lapse rate models with low-elevation temperature of 300 K (black line) and 295 K (dark gray line) and an empirical lapse rate (light gray line). $\Delta\delta^{18}O$ values were calculated using the modern low-elevation $\delta^{18}O$ value of −5.8‰ from New Delhi and a Miocene low-elevation $\delta^{18}O$ value of – 6‰ from Siwalik group paleosol carbonates. Uncorrected Miocene – Pleistocene water samples are indicated by diamonds and those that have been corrected for an ~ 3‰ post-industrial revolution increase are indicated by squares. In both cases the difference between Miocene – Pleistocene water and modern water $\delta^{18}O$ values is greater than the uncertainty associated with them indicating that the modeled loss in elevation is reliable.

for reconstructed water, they are relatively consistent with regards to differences in elevation (Δz), yielding an inter-model range of only 0.5 km.

The calculations above suggest that paleoelevations during the late Miocene were higher than those today, but they do not consider the effects of 20th century climate change. As noted above, the Siwalik paleosol record does not display any change in average $\delta^{18}O_{mw}$ values over the past ~ 8 Ma. However, the record does not cover the last ~ 100 years, a time of apparently major changes in $\delta^{18}O_{mw}$ water values in this region. Thompson and others (2000) noted a 3 permil increase in $\delta^{18}O$ values from the Dasuopu glacier in the Himalaya starting in the 20th century. This is consistent with, though larger than, increases observed at Dunde, Guliya and the Far East Rongbuk glaciers (Thompson and others, 1997, 2000; Kang and others, 2001) in the northeastern and northwestern Tibetan plateau and north-central Himalaya, respectively. As all applicable models have been developed with reference to the modern system, we add 3 permil to our reconstructed Miocene water values in order to compare them to modern water $\delta^{18}O$ values (fig. 13). Even with this correction the models still yield a minimum elevation decrease (mean elevation – uncertainty) between the Miocene and modern of *at least* 0.3, 0.4 and 0.5 km for the Rayleigh fractionation models with T_i = 295 K and T_i = 300 K and the empirically based curve, respectively. Again, comparing mean Miocene model elevations to modern model elevations predicts decreases of 0.6 (+ 0.2 – 0.3), 0.8 (± 0.3) and 0.8 (+ 0.3 - 0.4) km for the Rayleigh fractionation models with T_i = 295 K and T_i = 300 K and the

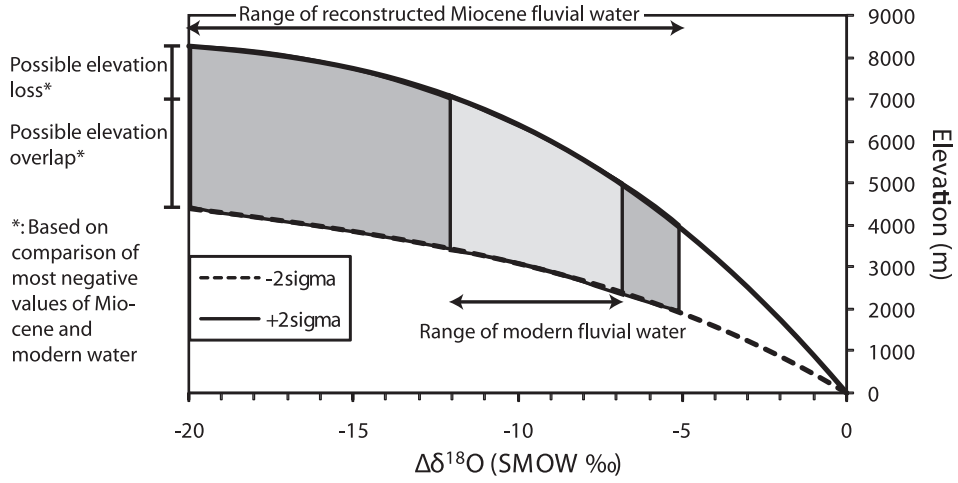

Fig. 14. Comparison of the range of $\Delta\delta^{18}O$ values for reconstructed Miocene fluvial water and modern water from the Zhada Basin versus elevation. Also shown is the 2σ uncertainty envelope around a mean $\Delta\delta^{18}O$ versus elevation lapse rate. The low elevation Ti for the mean $\Delta\delta^{18}O$ versus elevation lapse rate is 295K and low elevation relative humidity is 80%. Unlike figure 11, which presents a minimum uncertainty estimation, this figure presents the typically cited 2σ uncertainty. This results in considerable overlap in reconstructed elevation. However, it also admits the previously inferred elevation loss.

empirically based curve respectively. We caution that the addition of 3 permil to our Miocene $\Delta\delta^{18}O_{psw}$ may not be warranted, as interpretation of the glacial record remains unclear and the inferred increase in $\delta^{18}O_{mw}$ values may be due to a short-term, transitory change. However, as noted above, without the correction for changes in $\delta^{18}O_{mw}$ values of modern water, our estimates of paleoelevation would increase by $\sim$ 0.5 to 0.7 km.

The approach above results in a minimum estimation of paleoelevation uncertainty and deviates significantly from the approach to uncertainty estimation in previous paleoelevation studies. In order to facilitate comparison with previous paleoelevation studies, we compared the range of modern fluvial $\Delta\delta^{18}O_{sw}$ and Miocene fluvial $\Delta\delta^{18}O_{psw}$ values, uncertainties associated with those values, and typically cited model 2σ uncertainties (fig. 14). There is considerable overlap in $\Delta\delta^{18}O$ values. Elevated $\Delta\delta^{18}O_{psw}$ likely reflect evaporative enrichment and emphasize that the Miocene $\Delta\delta^{18}O_{psw}$ values are minimum estimates. Comparison of the most negative Miocene and modern $\Delta\delta^{18}O$ values indicates that there is $\sim$ 2.5 km of overlap in the possible paleoelevation estimates. However, the comparison also admits the previously inferred elevation loss of up to 1.2 km.

DISCUSSION AND CONCLUSIONS

Oxygen Isotopes from Zhada Basin

A key strength of this data set is substantial spatial and some temporal averaging of $\delta^{18}O_{cc}$ values in the shell samples. There is considerable noise in some oxygen isotope archives from the Tibetan Plateau, such as decadally resolved glacial ice, which would lead to a very large range in elevation estimates (for example, Thompson and others, 2000). However, water in which the fossil gastropods lived reflects the temporal and geographic average of multiple glaciers and precipitation events on many mountains surrounding the basin. Fine-scale temporal and spatial variations would be averaged in this process, accounting for the very consistent range of $\delta^{18}O_{cc}$ values we observe when

sorted by paleoenvironment (figs. 6 and 7). The $\delta^{18}O_{cc}$ record is consistent both across the basin and through millions of years, indicating that large-scale processes are the primary drivers.

We need to distinguish a precipitation $\delta^{18}O_{mw}$ signal from within the range of $\delta^{18}O_{cc}$ values, some of which have been influenced by post-precipitation evaporation, in order to interpret the $\delta^{18}O$ variability in the ancient record. $\delta^{18}O_{sw}$ values of water with low residence times (rivers or streams) are closest to $\delta^{18}O_{mw}$ values of rainfall, since there is the least opportunity for enrichment of $H_2{}^{18}O$ due to evaporation. $\delta^{18}O_{cc}$ values of gastropods from fluvial units therefore provide the most reliable record of the $\delta^{18}O_{mw}$ values of precipitation. The extremely low $\delta^{18}O_{cc}$ values imply low $\delta^{18}O_{mw}$ values and are due to the extreme elevation of mountains surrounding (and especially south of) Zhada Basin (Garzione and others, 2000b; Rowley and others, 2001). $\delta^{18}O_{psw}$ values (−12.8 to –24.3‰, VSMOW) are at least as low as $\delta^{18}O_{sw}$ values (−11.9 to −17.9‰), indicating that mountains surrounding the Zhada Basin were at elevations *at least* as high as today (>6,000m) during the late Miocene. Our paleoenvironmental modeling indicates that climate conditions similar to today prevailed in Zhada Basin during the late Miocene, suggesting an elevation decrease of ~0.6 to 0.8 km in the last 9 million years.

Extremely negative $\delta^{18}O_{cc}$ values of gastropods from fluvial intervals establish a baseline against which we can compare values from other intervals. The higher values, of between +0.7 and −8.2 permil (VPDB), of gastropods from lacustrine intervals are probably due to evaporative enrichment due to a longer residence time of average lake water (figs. 7 and 9). Calculated $\delta^{18}O_{psw}$ values from lacustrine intervals of between –2.2 and –11.7 permil (VSMOW) are at least as positive as results obtained from modern Tibetan lakes (+1.7 to -7.1‰, VSMOW, Gasse and others, 1991; Fontes and others, 1996; Quade, unpublished data), implying conditions at least as arid as today. The presence of gypsum and mudcracked layers within the lacustrine interval at Zhada, as well as Miocene dune fields support the conclusion that Zhada was arid in the Miocene. The arid conditions implied by both the isotopic and physical evidence provide additional support for an elevated Himalayan massif south of the Zhada Basin, insofar as orographic blockage of moisture in the region today makes it arid.

The shifts in gastropod $\delta^{18}O_{cc}$ and $\delta^{13}C_{cc}$ values correlate well with sediment accommodation creation, which also has a primary control on lithofacies and residence time of water. Gastropods from fluvial facies show the most negative $\delta^{18}O_{cc}$ values (figs. 6 and 7) and little covariance between $\delta^{18}O_{cc}$ and $\delta^{13}C_{cc}$ values (fig. 6), due to low water-residence times (Talbot, 1990; Li and Ku, 1997) in the basin. Although the discussion of $\delta^{18}O$ and $\delta^{13}C$ co-variance in closed basin lakes is usually based on trends in micrites, aquatic gastropods would also be expected to show similar co-variance because the controls on shell $\delta^{18}O$ and $\delta^{13}C$ are similar, the temperature, $\delta^{18}O$ and $\delta^{13}C$ of DIC (and secondarily algae) in the lake system (Aucour and others, 2003; Shanahan and others, 2005). Residence times were low because accommodation creation was low and water moved through the system quickly, resulting in $\delta^{18}O_{psw}$ values, which, like the modern, reflect the elevation of precipitation. Values from gastropods from supralittoral/marshy intervals fall between and overlap values from both fluvial and lacustrine intervals (fig. 7), indicating water residence times between that of fluvial and lacustrine facies. This increasing residence time is also reflected in the covariance between $\delta^{18}O_{cc}$ and $\delta^{13}C_{cc}$ values from samples from these intervals (fig. 6). Although the system was open at this point, the gradient was low, as suggested by marshy intervals. The increase in residence time is evidenced by higher $\delta^{18}O_{cc}$ values and $\delta^{18}O_{cc}$ and $\delta^{13}C_{cc}$ covariance. Samples from intermediate water-residence-time intervals continue the trend towards increasingly evolved $\delta^{18}O_{cc}$ and $\delta^{13}C_{cc}$ values. The samples still display covariance, but both the $\delta^{18}O_{cc}$ and $\delta^{13}C_{cc}$ values are systematically higher (figs. 6 and 7). As the rate of accommodation creation increased,

the basin closed, increasing the residence time of water as it began to pond and resulting in an increased evaporative effect. Gastropods from profundal lacustrine facies show uniformly high $\delta^{18}O_{cc}$ and $\delta^{13}C_{cc}$ values (figs. 6 and 7), due to water residence times which were long enough that the system was able to evolve to nearly a steady state (Li and Ku, 1997). Towards the top of the lacustrine interval the return to more negative $\delta^{18}O_{cc}$ values owes to the fact that the rate of accommodation creation was decreasing as the basin began to fill in (fig. 7).

Oxygen Isotopes from Zhongba

The water sampled from wetlands near Zhongba in May is enriched by between 10.3 and 15 permil with respect to that sampled in July. Samples 180506-4 and -5 have high $\delta^{18}O_{sw}$ and δD_{sw} values and fall off of the global meteoric water line, implying extensive evaporation. Only one sample, 260706-2 from the Tsangpo River, falls on the global meteoric water line. The rest of the samples fall on a mixing line defined by

$$\delta D = 4.035\ \delta^{18}O - 67.88 \quad (7)$$

between sample 270706-2 and samples 180506-4 and -5. The implication is that water in the wetlands is replenished during the summer monsoons and subsequently undergoes evaporation during the remainder of the year so that water sampled in May, just before the onset of the monsoon, is highly evaporatively enriched. Water sampled from the wetlands after the start of the monsoon (sample 260706-3) reflects replenishing and mixing between fresh fluvial water with low $\delta^{18}O_{sw}$ values and evaporated wetland water with high $\delta^{18}O_{sw}$ values.

Modeling shows that gastropod shell material in these open basin wetlands were most likely precipitated in equilibrium with monsoon wetland water at temperatures above MAT but no higher than the maximum average monthly temperature. Several conclusions can be drawn from these results. The first simply reiterates that summer monsoon water dominates the gastropod $\delta^{18}O_{cc}$ record from southern Tibet. This greatly simplifies the system because we can rule out significant contributions from alternative sources with unknown $\delta^{18}O_{mw}$ values and we can constrain the temperature of aragonite precipitation. Secondly, it means that the gastropod $\delta^{18}O_{cc}$ record is dominated by water that has been orographically lifted, and thus models based on that assumption (for example, Rowley and others, 2001) are valid. Finally, it means that high $\delta^{18}O_{cc}$ values imply closed basins. A basin that is even intermittently open, such as near Zhongba, will result in low $\delta^{18}O_{cc}$ values.

Carbon Isotopes

The increase in $\delta\ ^{13}C_{pm}$ values appears in two measured sections and can be confidently dated to the late Miocene, a time of global C_4 plant expansion (figs. 2 and 4). This large shift in $\delta^{13}C$ values (fig. 4) denotes a major increase in C_4 plants. $\delta\ ^{13}C$ values of organic matter from these results are also consistent with those seen in Neogene sections across the northern Indian sub-continent (Quade and others, 1989, 1995; France-Lanord and Derry, 1994; Ojha and others, 2000) and from the southern Tibetan Plateau (Garzione and others, 2000a; Wang and others, 2006). It is premature to use the presence or absence of C_4 biomass on the plateau to reconstruct paleoelevation as our knowledge of the modern distribution of C_4 plants on the plateau is incomplete. Though CAM plants have been reported on the Tibetan Plateau (for example, Lu and others, 2004), the plant remains from Zhada confirm that C_4 grasses, not CAM plants, are the cause of the late Miocene increase in $\delta\ ^{13}C_{pm}$ values in Zhada Basin. Moreover, several lines of evidence hint that C_4 plants are present at high elevations. Wang (2003), Garzione and others (2000a), and Wang and others (2008) found C_4 plants, particularly *Chenopodiaceae* and *Gramineae*, in the elevation range 3,000 to 4,800 m. These are the same families that dominate the pollen record of the Zhada

Formation (Li and Zhou, 2001). The limited ecosystem data published by Wang (2003) suggests that C_4 plants at high elevation prefer some sub-ecosystems, such as river valleys. More importantly, the fossil plants that we sampled in the Zhada Formation likely grew in or on the margins of the lake or along marshy watercourses leading to it, given their abundance and associated lithofacies. This suggests that the global expansion of C_4 grasses in the late Miocene was not limited to well-drained grasslands but also included semi-aquatic grasses in lakes and wetlands. Semi-aquatic C_4 grasses are well known in other riparian or wetland settings (for example, Jones, 1988; Martinelli and others, 1991), but, as far as we know, they remain unstudied in modern Tibet.

Application to Tectonic Models

This study suggests that the Zhada region of southwestern Tibet underwent a measurable decrease in elevation during the past 9 Myr, a result that is not specifically predicted in any existing tectonic model for the development of the Tibetan Plateau. The late Cenozoic structural setting of the Zhada region motivates us to invoke crustal thinning in response to mid- to upper-crustal extension (Zhang and others, 2000; Murphy and others, 2002; Murphy and Copeland, 2005; Thiede and others, 2006) as a mechanism that has contributed to elevation loss. However, future studies are needed to determine whether elevation loss was restricted to the Zhada region or affected a larger area of the plateau.

Conclusions

We have accounted for all the major controls of $\delta^{18}O$ change and still the lowest calculated $\delta^{18}O_{psw}$ is ~3.5 permil less than the most negative $\delta^{18}O_{sw}$ value of modern water. At this point, our ability to interpret the record in deep time based on the modern is better for oxygen than carbon isotopes, and we therefore favor the case for high elevations in southwestern Tibet at 9 Ma based on the oxygen isotope record. Future research in the region should focus on better understanding the controls and distribution of C_4 plants in all ecosystems in Tibet. Twentieth century climate changes can account for part, but not all of the difference between reconstructed and modern $\delta^{18}O_{sw}$ values, raising the intriguing possibility that mean catchment elevation in southwestern Tibet has decreased by 1 to 1.5 km since ~9 Ma. The decrease in elevation is indicated by an approach that assumes a minimum paleoelevation uncertainty estimate. While a solely climatically driven change in $\delta^{18}O_{sw}$ values cannot be completely ruled out, the proxies cited show no evidence of climate change which would result in the observed change. On the other hand, there is evidence of crustal thinning through detachment faulting in the Zhada area that could explain an elevation loss. This decrease in elevation is consistent with tectonic models that invoke collapse of an over-thickened Tibetan crust due to a change in internal or boundary conditions.

ACKNOWLEDGMENTS

The authors would like to thank Jeannette Saylor, Scott McBride and Cai Fulong for excellent assistance in the field. Thanks to Tank Ojha for assistance in the paleomagnetism lab at the University of Arizona. Thanks also to Majie Fan for assistance with carbonate, organic material and water analyses and useful discussions and E. Lindsay and X. Wang for identification of mammal fossils. This manuscript was significantly improved by reviews by Brian Currie, Carmala Garzione, and Peter Blisniuk. This research was supported by grants from ExxonMobil, Chevron-Texaco, the Galileo Circle of the University of Arizona, NSF Tectonics Program, and a grant from the National Natural Science Foundation of China (NSFC, 40625008).

Appendix

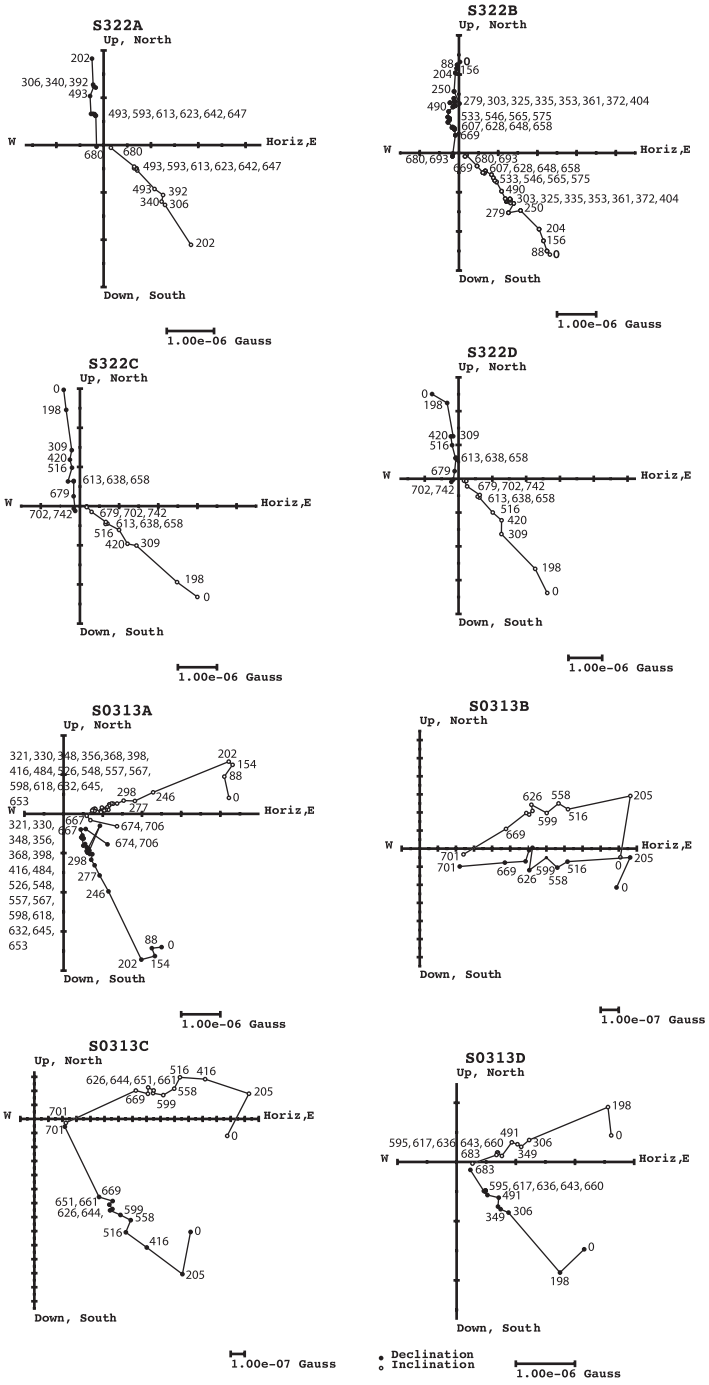

Fig. A1. Vector component diagrams for the South Zhada Sections. Site qualities A, B, C and D are presented by sites S322, S0313, LC6 and S0305 respectively.

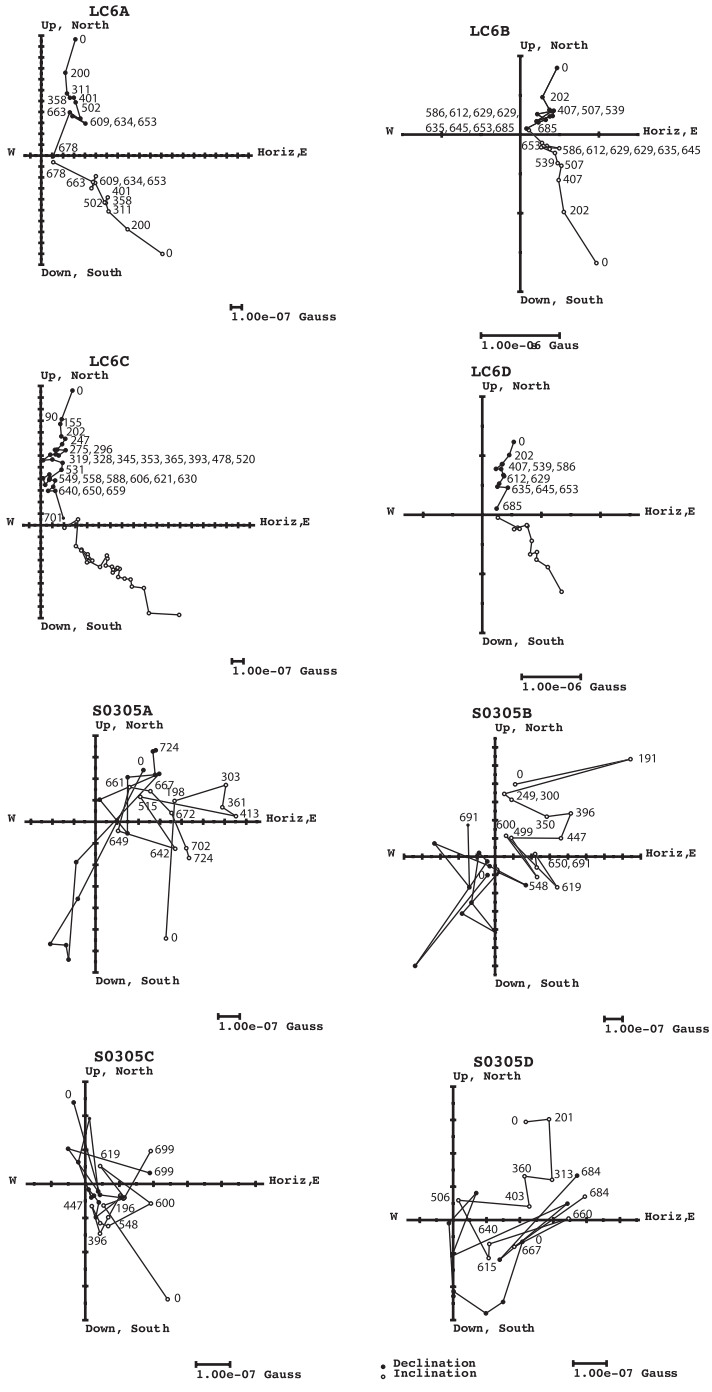

Fig. A1. (continued)

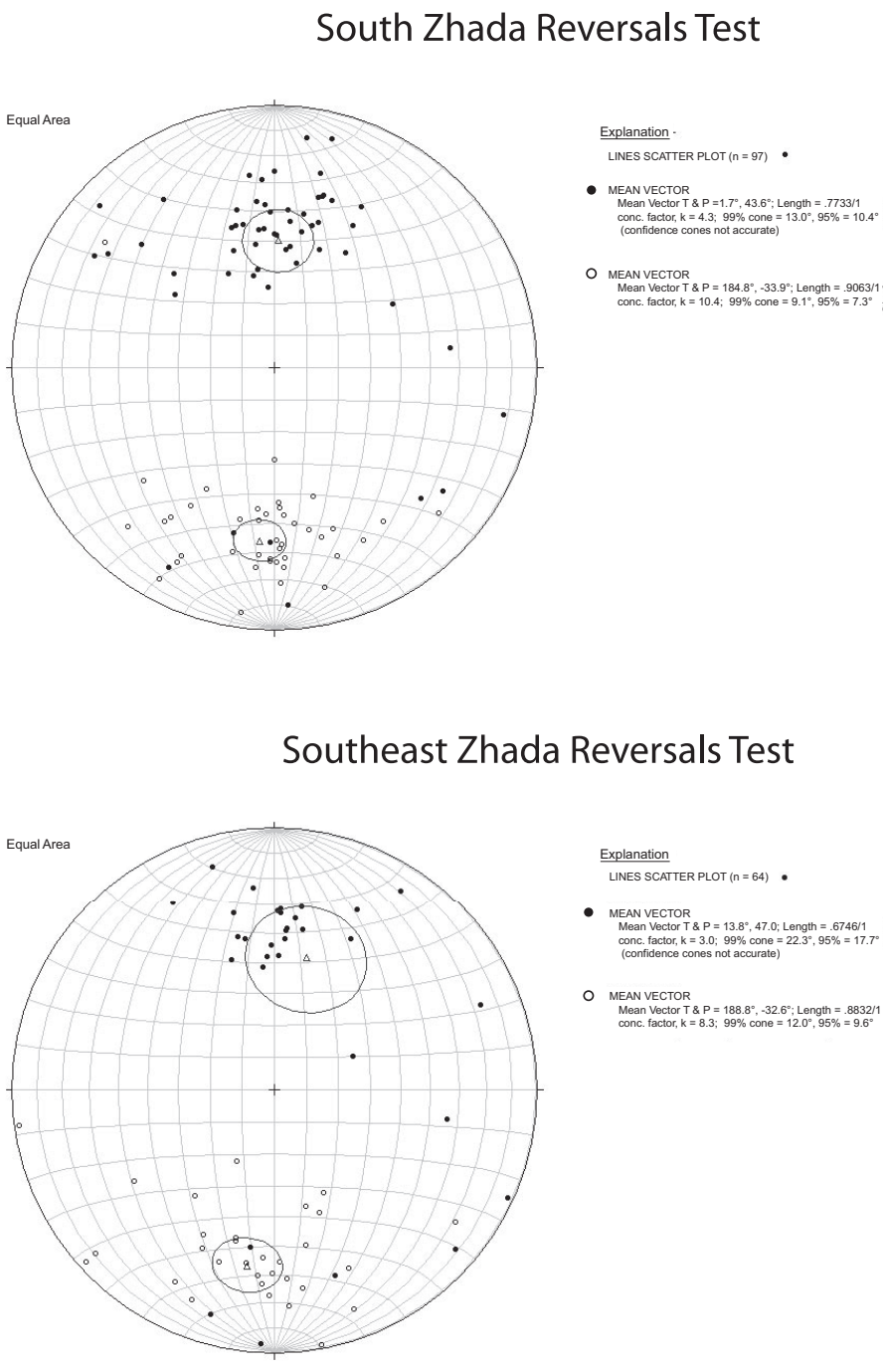

Fig. A2. Site mean and section mean vectors for the South Zhada and Southeast Zhada Sections. The mean vectors for normal and reversed polarity sites are anti-parallel and thus pass the "Reversals Test" (Butler, 1992).

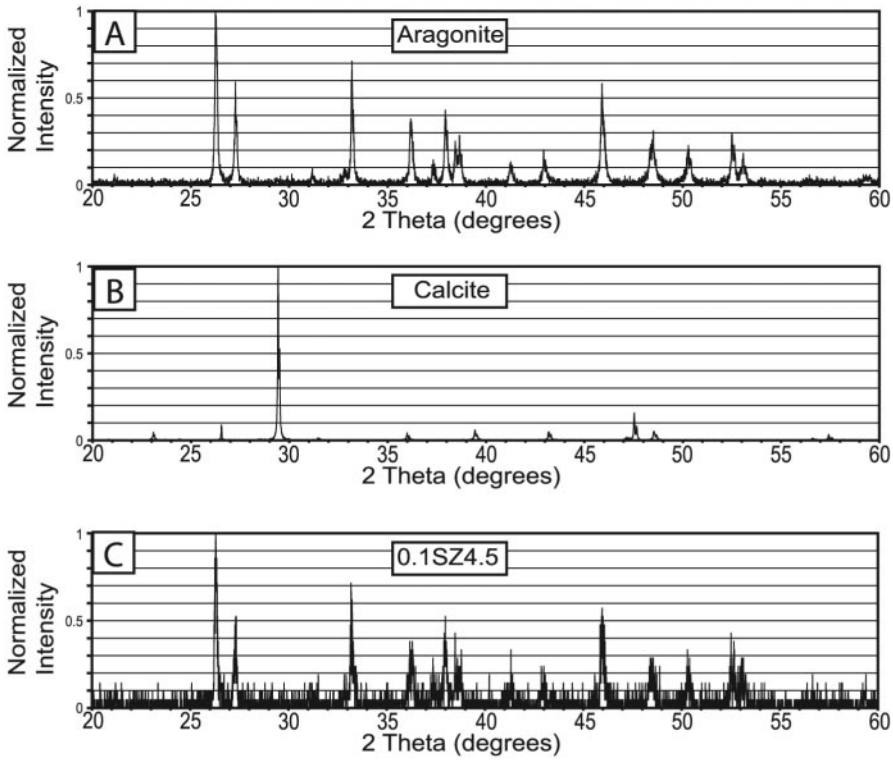

Fig. A3. X-Ray diffraction data for (A) aragonite standard, (B) calcite standard and (C) a representative sample from the South Zhada section. The sample matches peaks at 26−27°, 33°, 36−38°, 46°, 48.5°, 50° and 53° and lacks the prominent peak in calcite at 29.5°. Spectra from all samples that returned usable results (11 of 12) match the 0.1SZ4.5 spectrum.

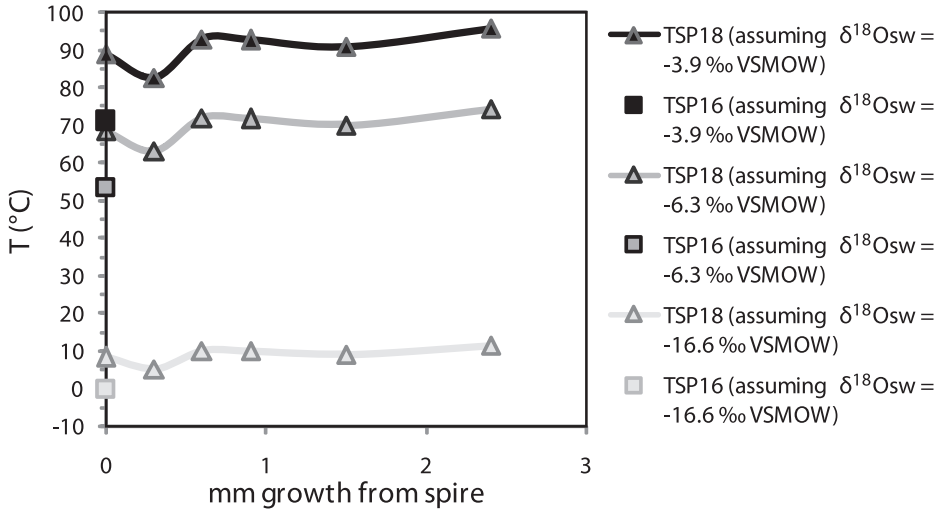

Fig. A4. Temperature of aragonite precipitation reconstructed based on modern gastropod shell $\delta^{18}O_{cc}$ and associated water $\delta^{18}O_{sw}$ values.

Table A1

Stable isotope and elevation data for modern water from the Zhada Basin and Zhongba area

Sample Name	Sample Elevation (m)	Maximum Watershed Elevation (m)	Mean Watershed Elevation (m)	$\delta^{18}O$ (‰ VSMOW)	δD (‰ VSMOW)	Lat. (N)	Long. (E)	Notes
Zhada water								
JQ-38	4325	5943.47	5188.63	-14.3	-106	31.53415	79.975603	Ai Shan
JQ-39	3613	6842.24	5419.08	-17.9	-130	31.46889	79.784636	Himalaya, Same Catchment as JQ-42 and w2571
JQ-40	3523	6856.46	4855.59	-14.3	-100	31.47474	79.74296	Sutlej River
JQ-37	4524	5843.2	5136.76	-16.1	-117	31.45092	80.12007	Ai Shan
JQ-41	3535	6856.46	4855.59	-16.5	-123	30.75320	79.77028	Sutlej River
JQ-42	3851	6842.24	5419.08	-16.4	-116	31.33770	79.790041	Himalaya, Same Catchment as JQ-39 and w2571
JQ-76	3988	5632	4547	-15.4	-117	31.3343	79.901867	Himalaya
JQ-77	3790	6856.46	4855.59	-14.4	-104	31.4005	79.921533	Sutlej River
JQ-80	4074	6253	4881	-13.4	-94	31.16668	80.0719	Himalaya
JQ-81	4101	5764	4844	-7.3	-75	31.12047	80.117783	Himalaya
JQ-82	4287	6179	5079	-15.7	-112	30.97107	80.3501	Himalaya
w0281	5184	6603.87	5768.95	-16.9	-125	31.13423	79.450681	Himalaya
w0381	3718	6856.46	4855.59	-15	-110	29.05971	88.000349	Sutlej River
w1771	4409	6043.34	5055.83	-16	-118	31.99252	79.642386	Ai Shan, Same location as 230706-3
w1772	4410	6257.3	5143.86	-15	-107	32.99252	80.642384	Ai Shan, Same location as 230706-4
w2371	4724	6069	5325	-13.2	-98	32.22481	79.57032	Ai Shan, Same location as 230706-2
w2571	3762	6842.24	5419.08	-17.6	-137	31.45323	79.657603	Himlaya, Same Catchment as JQ-39 and -42
110706-1	4678	5028	4760	-12.6	-90	31.30662	79.57273	Himalaya

Table A1
(continued)

Sample Name	Sample Elevation (m)	Maximum Watershed Elevation (m)	Mean Watershed Elevation (m)	$\delta^{18}O$ (‰ VSMOW)	δD (‰ VSMOW)	Lat. (N)	Long. (E)	Notes
160706-3	5026	6048.77	5454.95	-15	-112	31.19732	79.5518	Himalaya
160706-4	5042	5806.18	5304.09	-11.9	-86	31.20925	79.546983	Himalaya
200706-1	4341	6202.7	4998.89	-13.4	-99	31.88190	79.7102	Ai Shan
200706-2	4693	5352.13	4904.31	-13.5	-99	31.96550	79.755167	Ai Shan
200706-6	4431	6023	5063.87	-13.8	-100	32.20142	79.423383	Ai Shan
210706-1	4960	6081.74	5569.38	-12.7	-93	32.32415	79.0589	Ai Shan
230706-2	4738	6069	5325	-13.8	-101	32.23063	79.57265	Ai Shan, Same location as w2371
230706-3	4368	6043.34	5055.83	-13.4	-102	31.99842	79.64865	Ai Shan, Same location as w1771
230706-4	4368	6257.3	5143.86	-13.2	-102	31.99842	79.64865	Ai Shan, Same location as w1772
240706-1	4863	6255	5680	-14.3	-112	31.82573	79.03238	Ai Shan
240706-2	4534	6255	5510	-15.2	-108	31.91108	80.10542	Ai Shan
Zhongba water								
180506-4	4569			-6.3	-90	29.66257	84.16760	
180605-5	4591			-3.9	-86	29.08736	83.73856	
260706-2	4574			-18.9	-140	29.71140	84.07028	
260706-3	4571			-16.6	-140	29.68233	84.15037	

TABLE A2

Oxygen and carbon isotope data (VPDB) from Miocene – Pleistocene gastropods from Zhada Basin. Also included are the calculated Miocene – Pleistocene water values that the aragonite was precipitated in assuming a temperature of precipitation of 7°C and the stratigraphic height of the gastropod samples

Sample name	$\delta^{18}O$ (VPDB ‰)	$\delta^{18}O$ (VSMOW ‰)*	$\delta^{13}C$ (VPDB ‰)	Stratigraphic height (m)
South Zhada Section				
0.1SZ22A	-16.1	-19.0	-7.8	102.75
0.1SZ22B	-11.8	-14.7	-6.0	102.75
0.1SZ22C	-9.9	-12.8	-10.3	102.75
0.1SZ22D	-11.3	-14.2	-6.6	102.75
0.1SZ23.25	-20.9	-23.7	-7.7	104
0.1SZ24.5	-18.9	-21.8	-6.4	105.25
0.1SZ25	-10.5	-13.4	-6.2	105.75
0.1SZ25A	-10.2	-13.1	-5.7	105.75
0.1SZ26.2A	-20.2	-23.1	-7.6	106.95
0.1SZ26.2B	-21.0	-23.9	-5.4	106.95
0.1SZ26.2C	-21.4	-24.3	-7.0	106.95
0.1SZ29.7	-9.9	-12.8	-3.3	110.45
0.1SZ31A	-14.6	-17.4	-9.0	111.75
0.1SZ31B	-17.6	-20.5	-7.3	111.75
0.1SZ38.5	-14.2	-17.1	-8.5	119.25
0.1SZ4.5	-1.7	-4.6	-0.3	85.25
0.1SZ4.5AD1	-2.4	-5.4	0.7	85.25
0.1SZ4.5AD10	-2.2	-5.1	2.2	85.25
0.1SZ4.5AD10.1	-2.4	-5.3	1.9	85.25
0.1SZ4.5AD10.2	-3.5	-6.4	1.1	85.25
0.1SZ4.5AD11	-4.1	-7.0	0.4	85.25
0.1SZ4.5AD11.1	-3.9	-6.8	1.1	85.25
0.1SZ4.5AD12	-3.3	-6.2	1.9	85.25
0.1SZ4.5AD13	-3.5	-6.4	0.6	85.25
0.1SZ4.5AD14	-3.6	-6.5	1.7	85.25
0.1SZ4.5AD14.1	-3.1	-6.0	1.4	85.25
0.1SZ4.5AD14.2	-2.0	-4.9	1.4	85.25
0.1SZ4.5AD14.3	-4.7	-7.6	2.1	85.25
0.1SZ4.5AD15	-5.2	-8.1	2.6	85.25
0.1SZ4.5AD2	-3.4	-6.3	2.5	85.25
0.1SZ4.5AD4	-4.5	-7.4	2.1	85.25
0.1SZ4.5AD5	-3.1	-6.0	1.9	85.25
0.1SZ4.5AD6	-2.1	-5.0	1.9	85.25
0.1SZ4.5AD7	-1.8	-4.8	1.9	85.25
0.1SZ4.5AD8	-1.5	-4.4	3.0	85.25
0.1SZ4.5AD9	-1.8	-4.8	1.9	85.25
0.1SZ48.7	-13.6	-16.5	-5.1	129.45
0.1SZ52	-13.0	-15.9	-4.4	132.75
0.1SZ53.25	-17.3	-20.1	-3.2	134
0.1SZ53.25A	-20.3	-23.2	-6.5	134
0.1SZ53.25B	-21.6	-24.5	-7.3	134
0.1SZ53.25C	-5.2	-8.1	-5.7	134

Table A2
(continued)

Sample name	$\delta^{18}O$ (VPDB ‰)	$\delta^{18}O$ (VSMOW ‰)*	$\delta^{13}C$ (VPDB ‰)	Stratigraphic height (m)
0.1SZ53.25D	-18.3	-21.2	-7.1	134
0.2SZ10	-10.1	-12.9	0.7	160.7
0.2SZ11.5	-14.2	-17.0	-11.0	162.2
0.2SZ11.5A	-18.3	-21.2	-6.0	162.2
0.2SZ11.5B	-7.6	-10.5	-8.9	162.2
0.2SZ15.5	-9.1	-12.0	-11.2	166.2
0.2SZ20	-15.3	-18.2	-10.0	170.7
0.2SZ25	-11.7	-14.5	-4.1	175.7
0.2SZ36A	-17.7	-20.6	-10.6	186.7
0.2SZ36B	-17.0	-19.9	-7.8	186.7
0.3SZ15.15	-20.6	-23.5	-7.7	217.15
0.3SZ22	-8.1	-11.0	-2.5	224
0.3SZ32.5	-0.7	-3.6	-0.9	234.5
0.3SZ38.25	-5.6	-8.5	1.6	240.25
0.3SZ38.25D1	-8.3	-11.2	-2.8	240.25
0.3SZ38.25D2	-7.9	-10.8	-3.4	240.25
0.3SZ38.25D3	-7.0	-9.9	-3.7	240.25
0.3SZ38.25D4	-7.1	-10.0	-3.8	240.25
0.3SZ38.25D5	-6.8	-9.7	-2.9	240.25
0.3SZ38.25D6	-6.2	-9.1	-2.3	240.25
0.3SZ38.25D7	-7.1	-10.0	-2.6	240.25
0.3SZ38.25D8	-8.1	-11.0	-3.1	240.25
0.3SZ38.25D9	-8.8	-11.7	-3.3	240.25
0.3SZ42	-2.5	-5.4	-0.5	244
0.3SZ6.8AD2	-11.3	-14.2	-8.9	208.8
0.3SZ6.8ADA	-9.7	-12.6	-9.3	208.8
0.4SZ14.9	-20.3	-23.1	-9.4	278.25
0.4SZ24.65	-3.9	-6.8	-0.6	288
0.4SZ24.8	-4.5	-7.4	1.9	288.15
0.4SZ25	-0.9	-3.8	0.6	288.35
0.4SZ25.35	-1.8	-4.8	-3.0	288.7
0.4SZ4.8	0.2	-2.7	-1.3	268.15
1SZ12	-3.9	-6.8	-0.9	309.65
1SZ13	-12.5	-15.4	-3.0	310.65
1SZ13.8	-3.2	-6.1	-1.3	311.45
1SZ18	-1.8	-4.7	2.1	315.65
1SZ2.5	-2.4	-5.3	0.6	300.15
1SZ24	-5.4	-8.3	-0.2	321.65
1SZ24.1	-4.6	-7.5	-0.5	321.75
1SZ27.9	-2.8	-5.7	0.0	325.55
1SZ32	-1.5	-4.4	0.5	329.65
2SZ16.4	-12.1	-14.9	-5.1	349.5
2SZ3.25	-1.6	-4.5	0.8	336.35
2SZ34.5	-14.6	-17.4	-7.4	367.6
2SZ35.5	-11.6	-14.5	-5.3	368.6
2SZ41A	-13.9	-16.7	-2.6	374.1
2SZ41B	-17.4	-20.3	-5.1	374.1

Table A2
(continued)

Sample name	$\delta^{18}O$ (VPDB ‰)	$\delta^{18}O$ (VSMOW ‰)*	$\delta^{13}C$ (VPDB ‰)	Stratigraphic height (m)
2SZ41C	-14.6	-17.5	-5.5	374.1
2SZ43	-1.8	-4.8	0.9	376.1
2SZ43.1	-6.8	-9.7	-0.4	376.2
2SZ47	-1.9	-4.8	-0.6	380.1
2SZ51.5	-2.4	-5.3	-0.2	384.6
2SZ51.5AD0.5	-0.6	-3.5	-0.6	384.6
2SZ51.5AD10	-1.2	-4.1	0.2	384.6
2SZ51.5AD11	-2.1	-5.0	0.2	384.6
2SZ51.5AD12	-2.2	-5.1	0.1	384.6
2SZ51.5AD13	-2.1	-5.1	0.3	384.6
2SZ51.5AD14	-2.5	-5.4	0.2	384.6
2SZ51.5AD15	-0.8	-3.7	0.8	384.6
2SZ51.5AD3	-2.2	-5.1	-0.4	384.6
2SZ51.5AD4	-2.1	-5.0	-0.1	384.6
2SZ51.5AD5	-1.6	-4.5	0.3	384.6
2SZ51.5AD6	-0.8	-3.7	0.9	384.6
2SZ51.5AD7	-0.3	-3.2	0.0	384.6
2SZ51.5AD8	-0.3	-3.2	0.0	384.6
2SZ51.5AD9	-0.4	-3.3	-0.1	384.6
2SZ55	-2.3	-5.2	-0.7	388.1
2SZ7.5	-2.0	-4.9	1.0	340.6
3SZ0.15	-1.7	-4.6	0.9	389.25
3SZ14.45	-2.9	-5.8	1.9	403.55
3SZ14.5	-2.0	-4.9	1.2	403.6
3SZ18.5	-3.1	-6.0	-0.8	407.6
3SZ24	-2.2	-5.1	-0.3	413.1
3SZ24.1A	-2.8	-5.7	1.6	413.2
3SZ24.25A	-1.4	-4.4	0.8	413.35
3SZ24.25B	-1.8	-4.8	-1.1	413.35
3SZ24.25C	-1.6	-4.5	0.6	413.35
3SZ24.3	-2.0	-4.9	0.9	413.4
3SZ27	0.7	-2.2	-2.1	416.1
3SZ3.9	-2.0	-4.9	-0.4	393
3SZ32.5	-15.5	-18.3	-5.0	421.6
3SZ4	-3.3	-6.2	-0.8	393.1
3SZ41.5	-4.6	-7.5	0.4	430.6
3SZ49	-13.7	-16.6	-3.3	438.1
3SZ5	-1.4	-4.4	1.4	394.1
3SZ50.5	-1.0	-3.9	-1.2	439.6
3SZ55	-2.5	-5.4	1.2	444.1
3SZ61.8AD1	-0.8	-3.7	0.2	450.9
3SZ61.8AD2	-0.9	-3.8	0.1	450.9
3SZ62	-1.3	-4.2	0.0	451.1
3SZ67.5	-2.4	-5.3	0.9	456.6
3SZ74A	-3.0	-5.9	0.3	463.1
3SZ74B	-1.8	-4.7	0.1	463.1

Table A2
(continued)

Sample name	$\delta^{18}O$ (VPDB ‰)	$\delta^{18}O$ (VSMOW ‰)*	$\delta^{13}C$ (VPDB ‰)	Stratigraphic height (m)
3SZ75.6A	-5.0	-7.9	-0.5	464.7
3SZ75.6B	-4.6	-7.5	0.0	464.7
4SZ5	-9.9	-12.8	7.5	534.7
5SZ4.6A	-9.9	-12.8	1.3	642.9
5SZ4.6B	-7.7	-10.6	1.4	642.9
East Zhada Section				
1EZ10	-11.8	-13.6	-5.0	10
1EZ11	-18.3	-20.0	-8.9	11
1EZ12	-16.8	-18.6	-8.2	12
1EZ25.5	-12.7	-14.5	-4.4	25.5
1EZ25.5A	-16.1	-17.8	-4.1	25.5
1EZ25.5BD1	-9.7	-11.5	-5.4	25.5
1EZ25.5BD2	-9.3	-11.1	-5.6	25.5
1EZ25.5C	-7.9	-9.7	-5.3	25.5
1EZ25.5D	-15.6	-17.3	-5.8	25.5
1EZ27	-17.6	-19.3	-5.8	27
1EZ35.5	-15.1	-16.8	-8.0	35.5
1EZ42	-14.1	-15.8	-6.5	42
1EZ44.75	-16.9	-18.7	-10.8	44.75
1EZ46	-19.0	-20.8	-7.9	46
1EZ5.55	-14.4	-16.1	-6.8	5.55
1EZ5.55AD1	-17.8	-19.5	-9.1	5.55
1EZ5.55AD2	-18.7	-20.4	-9.1	5.55
1EZ5.55AD3	-19.2	-21.0	-9.6	5.55
1EZ5.55BD1	-13.5	-15.2	-6.9	5.55
1EZ5.55CD1	-11.6	-13.3	-5.2	5.55
1EZ5.55CD2	-11.2	-13.0	-5.6	5.55
1EZ52.2	-16.0	-17.8	-7.7	52.2
1EZ63	-10.7	-12.5	-4.0	63
1EZ8.9A	-15.8	-17.6	-12.8	8.9
1EZ8.9AD1	-16.7	-18.5	-6.8	8.9
1EZ8.9AD2	-17.1	-18.9	-12.8	8.9
1EZ8.9AD3	-17.2	-18.9	-12.4	8.9
1EZ8.9AD4	-17.6	-19.4	-12.7	8.9
1EZ8.9AD5	-18.2	-20.0	-11.8	8.9
1EZ8.9BD1	-19.0	-20.7	-12.9	8.9
1EZ8.9BD2	-18.9	-20.7	-12.0	8.9
1EZ8.9BD3	-16.1	-17.9	-13.4	8.9
1EZ8.9C	-17.5	-19.2	-13.6	8.9
2EZ111.5	-18.3	-20.1	-7.7	167
2EZ115.5	-17.1	-18.9	-5.5	171
2EZ16.2A	-13.5	-15.3	-12.4	71.7
2EZ16AD1	-15.6	-17.4	-7.5	71.5
2EZ16AD2	-13.3	-15.0	-3.8	71.5
2EZ16AD3	-4.9	-6.7	-1.8	71.5
2EZ16AD4	-15.8	-17.5	-3.0	71.5

Table A2
(continued)

Sample name	$\delta^{18}O$ (VPDB ‰)	$\delta^{18}O$ (VSMOW ‰)*	$\delta^{13}C$ (VPDB ‰)	Stratigraphic height (m)
2EZ16B	-16.5	-18.2	-11.1	71.5
2EZ22	-16.0	-17.8	-13.8	77.5
2EZ39	-19.1	-20.8	-8.1	94.5
2EZ60.7	-12.6	-14.3	-3.4	116.2
2EZ60.7A	-17.8	-19.6	-5.5	116.2
2EZ60.7B	-15.7	-17.4	-3.6	116.2
2EZ60.7C	-16.2	-18.0	-0.7	116.2
2EZ63	-11.7	-13.5	-0.3	118.5
2EZ63AD1	-10.9	-12.7	-5.0	118.5
2EZ63AD2	-11.1	-12.8	-5.4	118.5
2EZ63AD3	-11.9	-13.7	-6.5	118.5
2EZ63AD4	-11.5	-13.2	-6.7	118.5
2EZ63B	-6.9	-8.7	-2.7	118.5
2EZ63C	-11.6	-13.4	-3.5	118.5
2EZ63D	-8.8	-10.6	-3.2	118.5
2EZ63E	-12.2	-14.0	-8.7	118.5
2EZ89.45	-9.8	-11.6	-2.8	144.95
2EZ9.5	-14.3	-16.0	-4.6	65
3EZ100	-15.3	-17.1	-3.6	100
3EZ102	-16.5	-18.3	-3.5	276.35
3EZ119.5	-4.7	-6.5	-3.6	293.85
3EZ131.3A	-3.8	-5.6	0.0	305.65
3EZ131.3B	-2.5	-4.3	-0.2	305.65
3EZ136	-13.8	-15.6	-0.6	310.35
3EZ146	0.1	-1.7	-1.1	320.35
3EZ152.3A	-4.3	-6.0	-3.5	326.65
3EZ152.3B	-3.1	-4.9	-1.7	326.65
3EZ158	-2.8	-4.6	0.3	332.35
3EZ173	-3.7	-5.5	-0.2	347.35
3EZ180	-4.1	-5.9	0.1	354.35
3EZ180.5	-2.5	-4.3	0.4	354.85
3EZ183	-2.8	-4.6	-0.3	357.35
3EZ187.5	-9.3	-11.0	-2.2	361.85
3EZ46	-10.0	-11.8	-4.4	220.35
3EZ63.5	-15.7	-17.5	-5.0	237.85
3EZ69.2	-17.4	-19.1	-7.2	243.55
3EZ69.2A	-16.7	-18.5	-3.4	243.55
3EZ69.2BD1	-17.2	-18.9	-5.2	243.55
3EZ69.2BD2	-15.6	-17.3	-3.9	243.55
3EZ69.2C	-18.0	-19.7	-5.2	243.55
3EZ69.5	-16.0	-17.7	-5.9	243.85
3EZ7	-13.9	-15.7	-4.7	181.35
3EZ98	-14.1	-15.9	-3.8	272.35
3EZ99	-12.6	-14.3	-7.3	273.35
4EZ1	-3.0	-4.7	-2.7	414.45
4EZ23.9	-3.9	-5.7	0.3	437.35

Table A2
(continued)

Sample name	$\delta^{18}O$ (VPDB ‰)	$\delta^{18}O$ (VSMOW ‰)*	$\delta^{13}C$ (VPDB ‰)	Stratigraphic height (m)
4EZ23.9	-3.9	-5.7	1.3	437.35
4EZ23.9	-4.4	-6.2	1.0	437.35
4EZ23.9	-3.1	-4.9	0.5	437.35
4EZ23.9	-2.2	-4.0	1.3	437.35
4EZ23.9	-1.9	-3.7	1.7	437.35
4EZ23.9	-3.3	-5.1	1.0	437.35
4EZ23.9A EDGE	-4.2	-5.9	-0.2	437.35
4EZ23.9A APEX	-5.0	-6.8	-0.5	437.35
4EZ23.9B EDGE	-3.6	-5.4	-0.9	437.35
4EZ23.9B APEX	-5.3	-7.1	1.1	437.35
4EZ23.9C	-5.0	-6.8	0.7	437.35
4EZ23.9D	-2.0	-3.7	1.3	437.35
4EZ23.9E	-3.5	-5.3	-0.1	437.35
4EZ23.9 EDGE	-3.8	-5.6	1.1	437.35
4EZ23.9 APEX	-3.0	-4.8	1.3	437.35
4EZ23.9F	-2.5	-4.3	1.3	437.35
4EZ3	-3.6	-5.3	-1.8	416.45
4EZ30	-15.3	-17.0	-0.6	443.45
4EZ35.3	-10.8	-12.6	0.4	448.75
4EZ4	-3.1	-4.9	0.0	417.45
5EZ1.5A	-3.1	-4.9	-0.2	488.35
5EZ1.5B	-2.2	-4.0	-2.4	488.35
5EZ27.75	-3.2	-5.0	-0.2	514.6
5EZ3	-1.5	-3.3	-0.1	489.85
5EZ32	-4.8	-6.6	0.2	518.85
5EZ6.45	-4.4	-6.2	-1.1	493.3

*Assuming T = 7°C

TABLE A3

$\delta^{13}C$ (VPDB ‰) for plant material from the South Zhada and East Zhada sections

Sample Name	$\delta^{3}C$ (PDB ‰)	Stratigraphic height (m)
East Zhada Section		
1EZ5.55	-24.49	5.55
1EZ13	-23.93	13
1EZ34.1	-24.52	34.1
2EZ49.1	-24.80	104.65
2EZ68.5	-25.03	124.05
3EZ12.8	-23.41	150.25
3EZ139	-21.38	295.05
3EZ139	-24.07	295.05
3EZ147	-11.54	303.05
3EZ147	-18.53	303.05
3EZ90.8	-23.64	246.85
4EZ20	-23.39	371.55
4EZ3	-8.39	354.55
4EZ3	-23.24	354.55
4EZ6.4	-24.36	357.95
5EZ21.1	-14.24	421.05
5EZ35.6	-14.78	435.55
5EZ35.6	-11.97	435.55
5EZ39.9	-22.55	439.85
South Zhada Section		
0.1SZ25	-25.49	105.75
0.4SZ25	-14.80	288.36
0.4SZ25	-16.84	288.36
2SZ 50.35	-18.59	383.46
2SZ35.3	-24.16	368.41
2SZ7.7	-25.24	340.81
2SZ7.7	-24.8	340.81
2SZ5.85	-25.96	338.96
0.3SZ43.35	-18.68	245.36
0.3SZ32.6	-21.10	234.61
0.3SZ32	-22.97	234.01
0.3SZ32	-22.83	234.01
0.3SZ26	-24.24	228.01
0.1SZ52.35	-26.78	133.1
0.1SZ52.35	-26.08	133.1
0.1SZ25	-25.40	105.75
4SZ100.2	-24.05	629.9

References

Araguás-Araguás, L., Froehlich, K., and Rozanski, K., 1998, Stable isotope composition of precipitation over southeast Asia: Journal of Geophysical Research-Atmospheres, v. 103, No. D22, p. 28,721–28,742, doi:10.1029/98JD02582.

Armijo, R., Tapponnier, P., Mercier, J. L., and Han, T. L., 1986, Quaternary extension in southern Tibet: Field observations and tectonic implications: Journal of Geophysical Research-Solid Earth and Planets, v. 91, No. B14, p. 13,803-13,872, doi:10.1029/JB091iB14p13803.

Aucour, A. M., Sheppard, S. M. F., and Savoye, R., 2003, $\delta^{13}C$ of fluvial mollusk shells (Rhône River): A proxy for dissolved inorganic carbon?: Limnology and Oceanography, v. 48, p. 2186–2193.

Awashi, N., and Prasad, M., 1989, Siwalik plant fossils from Surai Khola area, western Nepal: Paleobotanist, v. 38, p. 298–318.

Beaumont, C., Jamieson, R. A., Nguyen, M. H., and Medvedev, S., 2004, Crustal channel flows: 1. Numerical models with applications to the tectonics of the Himalayan-Tibetan orogen: Journal of Geophysical Research-Solid Earth, v. 109, p. 29, doi:10.1029/2003JB002809.

Blisniuk, P. M., and Stern, L. A., 2005, Stable isotope paleoaltimetry: A critical review: American Journal of Science, v. 305, p. 1033–1074, doi:10.2475/ajs.305.10.1033.

Blisniuk, P. M., Hacker, B. R., Glodny, J., Ratschbacher, L., Bi, S. W., Wu, Z. H., McWilliams, M. O., and Calvert, A., 2001, Normal faulting in central Tibet since at least 13.5 Myr ago: Nature, v. 412, p. 628–632, doi:10.1038/35088045.

Butler, R., 1992, Paleomagnetism: magnetic domains to geologic terranes: Cambridge, Blackwell, 238 p.

Cande, S. C., and Kent, D. V., 1995, Revised calibration of the geomagnetic polarity timescale for the Late Cretaceous and Cenozoic: Journal of Geophysical Research-Solid Earth and Planets, v. 100, B4, p. 6093–6095, doi:10.1029/94JB03098.

Chamberlain, C. P., and Poage, M. A., 2000, Reconstructing the paleotopography of mountain belts from the isotopic composition of authigenic minerals: Geology, v. 28, p. 115–118, doi:10.1130/0091-7613(2000)28<115:RTPOMB>2.0.CO;2.

Chung, S., Lo, C., Lee, T., Zhang, Y., Xie, Y., Li, X., Wang, K., and Wang, P., 1998, Diachronous uplift of the Tibetan plateau starting 40 Myr ago: Nature, v. 394, p. 769–773, doi:10.1038/29511.

Currie, B. S., Rowley, D. B., and Tabor, N. J., 2005, Middle Miocene paleoaltimetry of southern Tibet: Implications for the role of mantle thickening and delamination in the Himalayan orogen: Geology, v. 33, p. 181–184, doi:10.1130/G21170.1.

Cyr, A. J., Currie, B. S., and Rowley, D. B., 2005, Geochemical evaluation of Fenghuoshan Group Lacustrine Carbonates, North-Central Tibet: Implications for the Paleoaltimetry of the Eocene Tibetan Plateau: Journal of Geology, v. 113, p. 517–533, doi:10.1086/431907.

DeCelles, P. G., Robinson, D. M., and Zandt, G., 2002, Implications of shortening in the Himalayan fold-thrust belt for uplift of the Tibetan Plateau: Tectonics, v. 21, No. 6, 1062, doi:10.1029/2001TC001322.

DeCelles, P. G., Quade, J., Kapp, P., Fan, M., Dettman, D. L., and Ding, L., 2007, High and dry in central Tibet during the Late Oligocene: Earth and Planetary Science Letters, v. 253, p. 389–401, doi:10.1016/j.epsl.2006.11.001.

Dettman, D. L., and Lohmann, K. C., 2000, Oxygen isotope evidence for high-altitude snow in the Laramide Rocky Mountains of North America during the Late Cretaceous and Paleogene: Geology, v. 28, p. 243–246, doi:10.1130/0091-7613(2000)28<243:OIEFHS>2.0.CO;2.

Dettman, D. L., Reische, A. K., and Lohmann, K. C., 1999, Controls on the stable isotope composition of seasonal growth bands in aragonitic fresh-water bivalves (unionidae): Geochimica et Cosmochimica Acta, v. 63, p. 1049–1057, doi:10.1016/S0016-7037(99)00020-4.

Dettman, D. L., Kohn, M. J., Quade, J., Ryerson, F. J., Ojha, T. P., and Hamidullah, S., 2001, Seasonal stable isotope evidence for a strong Asian monsoon throughout the past 10.7 m.y.: Geology, v. 29, p. 31–34, doi:10.1130/0091-7613(2001)029<0031:SSIEFA>2.0.CO;2.

Ding, L., Kapp, P., Zhong, D., and Deng, W., 2003, Cenozoic volcanism in Tibet: Evidence for a transition from oceanic to continental subduction: Journal of Petrology, v. 44, p. 1833–1865, doi:10.1093/petrology/egg061.

Ehleringer, J. R., Sage, R. F., Flanagan, L. B., and Pearcy, R. W., 1991, Climate change and the evolution of C_4 photosynthesis: Trends in Ecology and Evolution, v. 6, p. 95–99, doi:10.1016/0169-5347(91)90183-X.

Fontes, J. C., Gasse, F., and Gibert, E., 1996, Holocene environmental changes in Lake Bangong basin (Western Tibet). Part 1. Chronology and stable isotopes of carbonates of a Holocene lacustrine core: Palaeogeography, Palaeoclimatology, Palaeoecology, v. 120, p. 25–47, doi:10.1016/0031-0182(95)00032-1.

France-Lanord, C., and Derry, L. A., 1994, $\delta^{13}C$ of organic carbon in the Bengal Fan: Source evolution and transport of C3 and C4 plant carbon to marine sediments: Geochimica et Cosmochimica Acta, v. 58, p. 4809–4814, doi:10.1016/0016-7037(94)90210-0.

Ganser, A., 1964, Geology of the Himalayas: London, Wiley InterScience, 289 p.

Garzione, C. N., Dettman, D. L., Quade, J., DeCelles, P. G., and Butler, R. F., 2000a, High times on the Tibetan Plateau: Paleoelevation of the Thakkhola graben, Nepal: Geology, v. 28, p. 339–342, doi:10.1130/0091-7613(2000)28<339:HTOTTP>2.0.CO;2.

Garzione, C. N., Quade, J., DeCelles, P. G., and English, N. B., 2000b, Predicting paleoelevation of Tibet and the Himalaya from $\delta^{18}O$ vs. altitude gradients in meteoric water across the Nepal Himalaya: Earth and Planetary Science Letters, v. 183, p. 215–229, doi:10.1016/S0012-821X(00)00252-1.

Gasse, F., Arnold, M., Fontes, J. C., Fort, M., Gibert, E., Huc, A., Li, B. Y., Li, Y. F., Liu, Q., Melières, F., Vancampo, E., Wang, F. B., and Zhang, Q. S., 1991, A 13,000-year climate record from western Tibet: Nature, v. 353, p. 742–745, doi:10.1038/353742a0.

Gonfiantini, R., 1986, Environmental isotopes in lake studies, *in* Fritz, P., and Fontes, J., editors, Handbook of Environmental Isotope Geochemistry: The Terrestrial Environment, B: Amsterdam, Elsevier, p. 113–168.

Graham, S. A., Chamberlain, C. P., Yue, Y., Ritts, B. D., Hanson, A. D., Horton, T. W., Waldbauer, J. R., Poage, M. A., and Feng, X., 2005, Stable isotope records of Cenozoic climate and topography, Tibetan plateau and Tarim basin: American Journal of Science, v. 305, p. 101–118, doi:10.2475/ajs.305.2.101.

Grossman, E. L., and Ku, T., 1986, Oxygen and carbon isotope fractionation in biogenic aragonite: Temperature effects: Chemical Geology, v. 59, p. 59–74, doi:10.1016/0009-2541(86)90044-6.

Guynn, J. H., Kapp, P., Pullen, A., Heizier, M., Gehrels, G., and Ding, L., 2006, Tibetan basement rocks near Amdo reveal "missing" Mesozoic tectonism along the Bangong suture, central Tibet: Geology, v. 34, p. 505–508, doi:10.1130/G22453.1.

Harrison, T. M., Copeland, P., Kidd, W. S., and Yin, A., 1992, Raising Tibet: Science, v. 255, p. 1663–1670, doi:10.1126/science.255.5052.1663.

Jones, M. B., 1988, Photosynthetic responses of C_3 and C_4 wetland species in a tropical swamp: Journal of Ecology, v. 76, p. 253–262, doi:10.2307/2260467.

Jouzel, J., Alley, R. B., Cuffey, K. M., Dansgaard, W., Grootes, P., Hoffmann, G., Johnsen, S. J., Koster, R. D., Peel, D., Shuman, C. A., Stievenard, M., Stuiver, M., and White, J., 1997, Validity of the temperature reconstruction from water isotopes in ice cores: Journal of Geophysical Research-Oceans, v. 102, No.C12, p. 26,471–26,487, doi:10.1029/97JC01283.

Kang, S. C., Qin, D. H., Mayewski, P. A., Wake, C. P., and Ren, J. W., 2001, Climatic and environmental records from the Far East Rongbuk ice core, Mt. Qomolangma (Mt. Everest): Episodes, v. 24, p. 176–181.

Kapp, P., and Guynn, J. H., 2004, Indian punch rifts Tibet: Geology, v. 32, p. 993–996, doi:10.1130/G20689.1.

Kennett, J. P., 1985, The Miocene Ocean: Paleoceanography and Biogeography: Geological Society of America Memoir, p. i-vi, 1–337.

Kroon, D., Steens, T. N. F., and Troelstra, S. R., 1991, Onset of Monsoonal Related Upwelling in the Western Arabian Sea as Revealed by Planktonic Foraminifers: Proceedings of the Ocean Drilling Program: Scientific Results, v. 117, p. 257–263, doi:10.2973/odp.proc.sr.117.126.1991.

Li, F., and Li, D., 1990, Latest Miocene Hipparion (Plesiohipparion) of Zanda Basin, *in* Yang, Z., and Nie, Z., editors, Paleontology of the Ngari Area, Tibet (Xizang): Wuhan, China Geological University Press, p. 186–193.

Li, H.-C., and Ku, T.-L., 1997, $\delta^{13}C-\delta^{18}O$ covariance as a paleohydrological indicator for closed-basin lakes: Palaeogeography, Palaeoclimatology, Palaeoecology, v. 133, p. 69–80, doi:10.1016/S0031-0182(96)00153-8.

Li, J., and Zhou, Y., 2001, Palaeovegetation type analysis of the late Pliocene in Zanda basin of Tibet: Journal of Palaeogeography, v. 14, p. 52–58.

Li, T., Xiao, X., Li, G., Gao, Y., and Zhou, W., 1986, The crustal evolution and uplift mechanism of the Qinghai-Tibet plateau: Tectonophysics, v. 127, p. 279–289, doi:10.1016/0040-1951(86)90065-X.

Liu, D., 1981, Geological and ecological studies of Qinghai – Xizang Plateau, v. 2, Environment and Ecology of Qinghai-Xizang Plateau: Beijing, Science Press, 1163 p.

Lu, H. Y., Wu, N. Q., Gu, Z. Y., Guo, Z. T., Wang, L., Wu, H. B., Wang, G., Zhou, L. P., Han, J. M., and Liu, T. S., 2004, Distribution of carbon isotope composition of modern soils on the Qinghai-Tibetan Plateau: Biogeochemistry, v. 70, p. 273–297, doi:10.1023/B:BIOG.0000049343.48087.ac.

Majoube, M., 1971, Oxygen-18 and deuterium fractionation between water and steam: Journal de Chimie Physique et de Physico-Chimie Biologique, v. 68, p. 1423–1436.

Martinelli, L. A., Devol, A. H., Victoria, R. L., and Richey, J. E., 1991, Stable isotope variation in C_3 and C_4 plants along the Amazon River: Nature, v. 353, p. 57–59, doi:10.1038/353057a0.

McCaffrey, R., and Nabelek, J., 1998, Role of oblique convergence in the active deformation of the Himalayas and southern Tibet plateau: Geology, v. 26, p. 691–694, doi:10.1130/0091-7613(1998)026<0691:ROOCIT>2.3.CO;2.

Molnar, P., 2005, Mio-Pliocene growth of the Tibetan Plateau and evolution of East Asian climate: Palaeontologia Electronica, v. 8, p. 1–23.

Molnar, P., and Tapponnier, P., 1978, Active Tectonics of Tibet: Journal of Geophysical Research-Solid Earth and Planets, v. 83, No. B11, p. 5361–5375, doi:10.1029/JB083iB11p05361.

Molnar, P., England, P., and Martinod, J., 1993, Mantle Dynamics, uplift of the Tibetan Plateau, and the Indian Monsoon: Reviews of Geophysics, v. 31, p. 357–396, doi:10.1029/93RG02030.

Murphy, M. A., and Copeland, P., 2005, Transtensional deformation in the central Himalaya and its role in accommodating growth of the Himalayan orogen: Tectonics, v. 24, TC4012, doi:10.1029/2004TC001659.

Murphy, M. A., and Yin, A., 2003, Structural evolution and sequence of thrusting in the Tethyan fold-thrust belt and Indus-Yalu suture zone, southwest Tibet: Geological Society of America Bulletin, v. 115, p. 21–34, doi:10.1130/0016-7606(2003)115<0021:SEASOT>2.0.CO;2.

Murphy, M. A., Yin, A., Harrison, T. M., Durr, S. B., Chen, Z., Ryerson, F. J., Kidd, W. S. F., Wang, X., and Zhou, X., 1997, Did the Indo-Asian collision alone create the Tibetan plateau?: Geology, v. 25, p. 719–722, doi:10.1130/0091-7613(1997)025<0719:DTIACA>2.3.CO;2.

Murphy, M. A., Yin, A., Kapp, P., Harrison, T. M., Manning, C. E., Ryerson, F. J., Ding, L., and Guo, J., 2002, Structural evolution of the Gurla Mandhata detachment system, southwest Tibet: Implications for the eastward extent of the Karakoram fault system: Geological Society of America Bulletin, v. 114, p. 428–447. doi:10.1130/0016-7606(2002)114<0428:SEOTGM>2.0.CO;2.

NCDC, 2007, National Climatic Data Center, National Climatic Data Center.

Ojha, T. P., Butler, R. F., Quade, J., DeCelles, P. G., Richards, D., and Upreti, B. N., 2000, Magnetic polarity stratigraphy of the Neogene Siwalik Group at Khutia Khola, far western Nepal: Geological Society of America Bulletin, v. 112, p. 424–434, doi: 10.1130/0016-7606(2000)112<424:MPSOTN>2.0.CO;2.

Pearson, P. N., Ditchfield, P., and Shackleton, N. J., 2002, Palaeoclimatology - Tropical temperatures in greenhouse episodes - Reply: Nature, v. 419, p. 898−898, doi:10.1038/419898a.
Pilbeam, D., Morgan, M., Barry, J., and Flynn, L., 1996, European MN Units and the Siwalik Faunal Sequence of Pakistan, *in* Bernor, R. L., Fahlbusch, V., and Mittmann, H., editors, The Evolution of Western Eurasian Neogene Mammal Faunas: New York, Columbia University Press, p. 96–105.
Poage, M. A., and Chamberlain, C. P., 2001, Empirical relationships between elevation and the stable isotope composition of precipitation and surface waters: Considerations for studies of paleoelevation change: American Journal of Science, v. 301, p. 1–15, doi:10.2475/ajs.301.1.1.
Prell, W. L., and Kutzbach, J. E., 1992, Sensitivity of the Indian monsoon to forcing parameters and implications for its evolution: Nature, v. 360, p. 647–652, doi:10.1038/360647a0.
Prell, W., Murray, D., Clemens, S., and Anderson, D., 1992, Evolution and variability of the Indian Ocean summer monsoon: evidence from the western Arabian Sea drilling program, *in* Duncan, R., editor, Synthesis of Results from the Scientific Drilling of the Indian Ocean: Washington, D.C., AGU, p. 447–469.
Quade, J., Cerling, T. E., and Bowman, J. R., 1989, Development of Asian monsoon revealed by marked ecological shift during the latest Miocene in northern Pakistan: Nature, v. 342, p. 163–166, doi:10.1038/342163a0.
Quade, J., Cater, J. M. L., Ojha, T. P., Adam, J., and Harrison, T. M., 1995, Late Miocene environmental change and in Nepal and the northern Indian subcontinent; stable isotopic evidence from paleosols: Geological Society of America Bulletin, v. 107, p. 1381–1397, doi:10.1130/0016-7606(1995)107<1381:LMECIN>2.3.CO;2.
Ratschbacher, L., Frisch, W., Liu, G., and Chen, C., 1994, Distributed deformation in southern and western Tibet during and after the India-Asian collision: Journal of Geophysical Research-Solid Earth and Planets, v. 99, B10, p. 19917–19945, doi:10.1029/94JB00932.
Raymo, M. E., and Ruddiman, W. F., 1992, Tectonic forcing of Late Cenozoic climate: Nature, v. 359, p. 117–122, doi:10.1038/359117a0.
Rowley, D., and Currie, B., 2006, Palaeo-altimetry of the late Eocene to Miocene Lunpola basin, central Tibet: Nature, v. 439, p. 677–681, doi:10.1038/nature04506.
Rowley, D. B., and Garzione, C. N., 2007, Stable Isotope-Based Paleoaltimetry: Annual Review of Earth and Planetary Sciences, v. 35, p. 463–508, doi:10.1146/annurev.earth.35.031306.140155.
Rowley, D. B., Pierrehumbert, R. T., and Currie, B. S., 2001, A new approach to stable isotope-based paleoaltimetry: implications for paleoaltimetry and paleohypsometry of the High Himalaya since the Late Miocene: Earth and Planetary Science Letters, v. 188, p. 253–268, doi:10.1016/S0012-821X(01)00324-7.
Rozanski, K., Araguas-Araguas, L., and Gonfiantini, R., 1993, Isotopic patterns in modern global precipitation, *in* Swart, P., Lohman, K., McKenzie, J., and Savin, S., editors, Climate Change in Continental Isotopic Records - Geophysical Monograph 78: Washington, D.C., American Geophysical Union, p. 1–36.
Ruddiman, W., Raymo, M., Prell, W., and Kutzback, J., 1997, The uplift-climate connection: A synthesis, *in* Ruddiman, W. F., editor, Tectonic Uplift and climate change: New York, Plenum Press, p. 471–515.
Sarkar, S., 1989, Siwalik pollen succession from Surai Khola of western Nepal and its reflection on paleoecology: Paleobotanist, v. 38, p. 319–324.
Savin, S. M., Abel, L. J., Barrera, E., Hodell, D., Keller, G., Kennett, J. P., Killingley, J., Murphy, M., and Vincent, E., 1985, The evolution of Miocene surface and near-surface marine temperatures: oxygen isotopic evidence, *in* Kennett, J. P., editor, The Miocene Ocean: Paleoceanography and Biogeography: Geological Society of America Memoir, #163, p. 49–82.
Seeber, L., and Pecher, A., 1998, Strain partitioning along the Himalayan arc and the Nanga Parbat antiform: Geology, v. 26, p. 791–794, doi:10.1130/0091-7613(1998)026<0791:SPATHA>2.3.CO;2.
Shanahan, T. M., Pigati, J. S., Dettman, D. L., and Quade, J., 2005, Isotopic variability in the aragonite shells of freshwater gastropods living in springs with nearly constant temperature and isotopic composition: Geochimica et Cosmochimica Acta, v. 69, p. 3949–3966, doi:10.1016/j.gca.2005.03.049.
Siegenthaler, U., and Oeschger, H., 1980, Correlation of ^{18}O in precipitation with temperature and altitude: Nature, v. 285, p. 314–317, doi:10.1038/285314a0.
Spicer, R. A., Harris, N. B. W., Widdowson, M., Herman, A. B., Guo, S., Valdes, P. J., Wolfe, J. A., and Kelley, S. P., 2003, Constant elevation of southern Tibet over the past 15 million years: Nature, v. 421, p. 622–624, doi:10.1038/nature01356.
Stewart, D. R. M., Pearson, P. N., Ditchfield, P. W., and Singano, J. M., 2004, Miocene tropical Indian Ocean temperatures: evidence from three exceptionally preserved foraminiferal assemblages from Tanzania: Journal of African Earth Sciences, v. 40, p. 173–190, doi:10.1016/j.jafrearsci.2004.09.001.
Talbot, M. R., 1990, A review of the paleohydrological interpretation of carbon and oxygen isotopic ratios in primary lacustrine carbonates: Chemical Geology, v. 80, p. 261–279.
Tapponnier, P., Xu, Z. Q., Roger, F., Meyer, B., Arnaud, N., Wittlinger, G., and Yang, J. S., 2001, Geology - Oblique stepwise rise and growth of the Tibet Plateau: Science, v. 294, p. 1671–1677, doi:10.1126/science.105978.
Taylor, M., Yin, A., Ryerson, F. J., Kapp, P., and Ding, L., 2003, Conjugate strike-slip faulting along the Bangong-Nujiang suture zone accommodates coeval east-west extension and north-south shortening in the interior of the Tibetan Plateau: Tectonics, v. 22, 1044, doi:10.1029/2002TC001361, 2003.
Thiede, R. C., Arrowsmith, J. R., Bookhagen, B., McWilliams, M., Sobel, E. R., and Strecker, M. R., 2006, Dome formation and extension in the Tethyan Himalaya, Leo Pargil, northwest India: Geological Society of America Bulletin, v. 118, p. 635–650, doi:10.1130/B25872.1.
Thompson, L. G., Yao, T., Davis, M. E., Henderson, K. A., Mosley-Thompson, E., Lin, P. N., Beer, J., Synal, H. A., Cole-Dai, J., and Bolzan, J. F., 1997, Tropical climate instability: The last glacial cycle from a Qinghai-Tibetan ice core: Science, v. 276, p. 1821–1825, doi: 10.1126/science.276.5320.1821.

Thompson, L. G., Yao, T., Mosley-Thompson, E., Davis, M. E., Henderson, K. A., and Lin, P. N., 2000, A high-resolution millennial record of the South Asian Monsoon from Himalayan ice cores: Science, v. 289, p. 1916–1919, doi:10.1126/science.289.5486.1916.

Tian, L., Yao, T., Numaguti, A., and Sun, W., 2001, Stable isotope variations in monsoon precipitation on the Tibetan Plateau: Journal of the Meteorological Society of Japan, v. 79, p. 959–966, doi:10.2151/jmsj.79.959.

Turner, S., Hawkesworth, C., Liu, J., Rogers, N., Kelley, S., and van Calsteren, P., 1993, Timing of Tibetan uplift constrained by analysis of volcanic rocks: Nature, v. 364, p. 50–54, doi:10.1038/364050a0.

Wang, J. H., Yin, A., Harrison, T. M., Grove, M., Zhang, Y. Q., and Xie, G. H., 2001, A tectonic model for Cenozoic igneous activities in the eastern Indo-Asian collision zone: Earth and Planetary Science Letters, v. 188, p. 123–133, doi:10.1016/S0012-821X(01)00315-6.

Wang, R. Z., 2003, C_4 plants in the vegetation of Tibet, China: Their natural occurrence and altitude distribution pattern: Photosynthetica, v. 41, p. 21–26, doi:10.1023/A:1025844009120.

Wang, S. F., Zhang, W. L., Fang, X. M., Dai, S., and Kempf, O., 2008a, Magnetostratigraphy of the Zanda basin in southwest Tibet Plateau and its tectonic implications: Chinese Science Bulletin, v. 53, p. 1393–1400, doi:10.1007/s11434-008-0132-9.

Wang, Y., Deng, T., and Biasatti, D., 2006, Ancient diets indicate significant uplift of southern Tibet after ca. 7 Ma: Geology, v. 34, p. 309–312, doi:10.1130/G22254.1.

Wang, Y., Kromhout, E., Zhang, C., Xu, Y., Parker, W., Deng, T., and Qiu, Z., 2008b, Stable isotopic variations in modern herbivore tooth enamel, plants and water on the Tibetan Plateau: Implications for paleoclimate and paleoelevation reconstructions: Palaeogeography, Palaeoclimatology, Palaeoecology, v. 260, p. 359–374, doi:10.1016/j.palaeo.2007.11.012.

Williams, M., Haywood, A. M., Taylor, S. P., Valdes, P. J., Sellwood, B. W., and Hillenbrand, C. D., 2005, Evaluating the efficacy of planktonic foraminifer calcite $\delta^{18}O$ data for sea surface temperature reconstruction for the Late Miocene: Geobios, v. 38, p. 843–863, doi:10.1016/j.geobios.2004.12.001.

Woodburne, M. O., Bernor, R. L., and Swisher, C. C., III, 1996, An appraisal of the stratigraphic and phylogenetic bases for the "Hipparion" Datum in the Old World, *in* Bernor, R. L., Fahlbusch, V., and Mittmann, H., editors, The evolution of western Eurasian Neogene mammal faunas: New York, Columbia University Press, p. 124–136.

Yin, A., Harrison, T. M., Murphy, M. A., Grove, M., Nie, S., Ryerson, F. J., Feng, W. X., and Le, C. Z., 1999, Tertiary deformation history of southeastern and southwestern Tibet during the Indo-Asian collision: Geological Society of America Bulletin, v. 111, p. 1644–1664, doi:10.1130/0016-7606(1999)111<1644:TDHOSA>2.3.CO;2.

Zachos, J., Pagani, M., Sloan, L., Thomas, E., and Billups, K., 2001, Trends, rhythms, and aberrations in global climate 65 Ma to present: Science, v. 292, p. 686–693, doi:10.1126/science.1059412.

Zachos, J. C., Arthur, M. A., Bralower, T. J., and Spero, H. J., 2002, Palaeoclimatology - Tropical temperatures in greenhouse episodes: Nature, v. 419, p. 897–898, doi:10.1038/419897b.

Zhang, J., Ding, L., Zhong, D., and Zhou, Y., 2000, Orogen-parallel extension in Himalaya: Is it the indicator of collapse or the product in process of compressive uplift?: Chinese Science Bulletin, v. 45, p. 114–120, doi:10.1007/BF02884653.

Zhang, Q., Wang, F., Ji, H., and Huang, W., 1981, Pliocene sediments of the Zanda basin, Tibet: Journal of Stratigraphy, v. 5, p. 216–220.

Zheng, H., Powell, C. M., An, Z., Zhou, J., and Dong, G., 2000, Pliocene uplift of the northern Tibetan Plateau: Geology, v. 28, p. 715–718, doi:10.1130/0091-7613(2000)28<715:PUOTNT>2.0.CO;2.

Zhisheng, A., Kutzbach, J. E., Prell, W. L., and Porter, S. C., 2001, Evolution of Asian monsoons and phased uplift of the Himalayan Tibetan plateau since Late Miocene times: Nature, v. 411, p. 62–66, doi:10.1038/35075035.